Fully printed potentiometric pH sensor

By

Shirin MAHINNEZHAD

THESIS PRESENTED TO ÉCOLE DE TECHNOLOGIE SUPÉRIEURE IN PARTIAL FULFILLEMENT FOR A DEGREE OF MASTER'S WITH THESIS IN ENGINEERING WITH A PERSONALIZED CONCENTRATION
M. SC. A.

MONTREAL, JANUARY 31, 2023

ÉCOLE DE TECHNOLOGIE SUPÉRIEURE
UNIVERSITÉ DU QUÉBEC

BOARD OF EXAMINERS

THIS THESIS HAS BEEN EVALUATED

BY THE FOLLOWING BOARD OF EXAMINERS

Mr. Ricardo Izquierdo, Thesis Supervisor
Department of Electrical Engineering, École de technologie supérieure

Mr. Andy Shih, Thesis Co-supervisor
Department of Electrical Engineering, École de technologie supérieure

Ms. Kuljeet Kaur, President of the Board of Examiners
Department of Electrical Engineering, École de technologie supérieure

Mr.Qingson Wang , Member of the jury
Department of Electrical Engineering, École de technologie supérieure

THIS THESIS WAS PRENSENTED AND DEFENDED

IN THE PRESENCE OF A BOARD OF EXAMINERS AND PUBLIC

JANUARY 09, 2023

AT ÉCOLE DE TECHNOLOGIE SUPÉRIEURE

ACKNOWLEDGMENT

I would like to express my sincere gratitude to my advisor, Pr. Ricardo Izquierdo at École de technologie supérieure (ETS). I am grateful for all his support and guidance during my research. He helped and motivated me to explore his interesting research area. I am also grateful to have the consistent help and support from my co-supervisor, Pr. Andy Shih at École de technologie supérieure (ETS). He helped me to think deeply with different points of view facing the challenges in my project and he helped me to present my research.

I would like to extend special thanks to the technical staff at ETS, especially Mr. Normand Gravel, who helped me a lot in learning the required tools. I would like to also express my gratitude to all of my research team colleagues.

I would like to thank my dear spouse, Mohsen, who has always helped and supported me during my studies with his endless patience and kindness.

Finally, I am grateful to my wonderful parents and my adorable sister who always motivate and support me in the path I choose.

CAPTEUR DE PH POTENTIOMÉTRIQUE ENTIÈREMENT IMPRIMÉ

Shirin MAHINNEZHAD

RESUME

Récemment, il y a une croissance exceptionnelle de la recherche liée au développement de capteurs flexibles pour l'analyse de la santé. Les mesures de pH peuvent être effectuées de manière non invasive et continue, ce qui en fait un excellent paramètre pour surveiller les différentes étapes de la cicatrisation des plaies. Ici, nous rapportons la fonctionnalité pH d'un composite polyaniline/graphite (PANI/G) dans un capteur de pH potentiométrique entièrement imprimé et l'effet de la charge de graphite sur la fonctionnalité du capteur. Des composites PANI/G dans différents rapports ont été imprimés par jet d'aérosol sur Ag/AgCl avec et sans couche de graphite comme électrode de travail dans un capteur potentiométrique à deux électrodes sur un substrat flexible. Le rôle de la couche de graphite sur l'électrode de travail dans la fonctionnalité du capteur a été étudié. Les composites PANI/G ont été préparés par une méthode de traitement en solution utilisant une pâte de graphite et une poudre de sel de polyaniline émeraude. Les échantillons ont été caractérisés par analyse XRD, SEM et FTIR pour étudier les relations entre les relations physiques et chimiques et les performances des capteurs. Les capteurs ont été testés dans la gamme de pH de 3 à 10, présentant une sensibilité linéaire, stable et proche de Nernst de 53 mV/pH et un temps de réponse de 15 s.

Mots-clés — capteur de pH ; graphite; polyaniline; capteur potentiométrique ; impression d'écran; impression par jet d'aérosol; électronique imprimée

FULLY PRINTED POTENTIOMETRIC PH SENSOR

Shirin MAHINNEZHAD

ABSTRACT

Recently, there has been an exceptional growth in research related to the development of flexible sensors for health monitoring and analysis. In particular, pH measurements can be done non-invasively and continuously, making it an excellent parameter for monitoring different stages of wound healing. Here, we report pH sensitivity of a polyaniline/graphite (PANI/G) composite in a fully-printed potentiometric pH sensor and the effect of graphite loading on sensor performance. PANI/G composites in different ratios were aerosol-jet printed on Ag/AgCl with and without a graphite layer as the working electrode in a two-electrode potentiometric sensor on a flexible substrate. The role of the graphite layer on the working electrode has been investigated. PANI/G composites were prepared by a solution processing method using a graphite paste and polyaniline emeraldine salt powder. Samples were characterized by x-ray diffraction, scanning electron microscopy, and Fourier-transform infrared spectroscopy analysis to investigate the relations between the physical and chemical components and the performance of the sensors. The sensors were tested in the pH range from 3 to 10, exhibiting a linear, stable and near-Nernstian sensitivity of 53 mV/pH and a response time of 15 s.

Keywords — pH sensor; graphite; polyaniline; potentiometric sensor; screen printing; aerosol-jet printing; printed electronics

TABLE OF CONTENTS

LIST OF TABLES

Page

LIST OF FIGURES

Page

LIST OF ABREVIATIONS

G	Graphite
PANI	Polyaniline
PANI (ES)	Polyaniline (emeraldine salt)
PANI (EB)	Emeraldine base (EB; half oxidized form)
EMF	Electromotive force
RE	Reference electrode
WE	Working electrode
PET	polyethylene terephthalate
NMP	N- methyl-2-pyrrolidone
SEM	Scanning Electron Microscopy
FTIR	Fourier transform infrared
XRD	X-Ray diffraction analysis
IoT	Internet of things
AJP	Aerosol-Jet Printing

INTRODUCTION

Printed electronics technologies enable the fabrication of the many electronic devices, including printed pH sensors, using potentially biocompatible and biodegradable organic materials. Printed technologies further enable the fabrication of electronic devices and sensors on low temperature and flexible substrates. For example, printed and flexible pH sensors can be integrated in applications such as smart bandage systems for remote wound monitoring where skin pH is an indicator for wound healing (Park et al. 2019a). Measuring and analyzing pH values of a solution is also vital for assessing different biochemical and biological processes in various industries, from medical devices to food packaging systems (Chu et al. 2015; Gao et al. 2016; Nyein et al. 2016). To build printed pH sensors, careful design of the structure, fabrication process and organic sensing material is required. On the latter, organic semiconductors are widely utilized in electrochemical sensors, and particularly in pH sensing applications because of their excellent electrical conductivity, low cost, availability, and versatility for functionalization (Kahlert 2008).

In this work, a fully-printed potentiometric pH sensor based on graphite/polyaniline nanocomposites is presented with near-Nernstian sensitivity. The challenge of obtaining a suitable sensing material in terms of physical properties such as a viscosity that is compatible with screen printing has been investigated. With a large portion of electronic sensors fabricated with a mix of printing and standard microfabrication processes, a fully printed pH sensor was targeted with its own fabrication challenges. Furthermore, in order to explore the effects of different ratios of graphite and polyaniline on the sensor performance, aerosol-jet printing was used further to modify the working electrode for enhanced performance. In chapter 1, a literature review on the different types of pH sensors and printing technologies is presented. Chapter 2 consists of the materials preparation and fabrication process of the printed pH sensors. Chapter 3 describes the characterization and testing methods used. Finally, chapter 4 presents the results and analysis of the sensors' performance.

CHAPTER 1

LITERATURE REVIEW

1.1 Printed pH Sensors

There are two classifications of sensors: physical and chemical, based on their operating principle. In physical sensors, physical parameters such as temperature, pressure, and flow rate are measured and converted into an electrical signal via processes such as thermoelectric, photoelectric, magnetoelectric, and piezoelectric. On the other hand, a chemical reaction between the sensor's active material and the targeted chemical species (whether in liquid or gaseous state) is the basis for chemical sensors. These ascertain the chemical information of the targeted analyte and convert it into a signal that can be measured and used for analysis. A chemical sensor typically consists of two fundamental parts: a receptor that recognizes analyte molecules present on the surface of the active materials and a transducer that converts the chemical reaction to an electrical signal. Adsorption, ion exchange, and liquid-liquid interaction are all interaction processes used in chemical sensors. These phenomena operate at the interface between the analyte and the receptor's surface, changing the receptor's physical characteristics such that the combined transducers can pick up an electrical signal. Electrochemical, optical, mass, and heat-sensitive sensors are different subcategories of chemical sensors (Douglas and Eaton 2002).

pH sensors are an important class of chemical sensors. Measuring pH values for the acidity and alkalinity of a solution is used as one of the parameters for assessing biochemical and biological processes in different industries such as biomedical devices and food packaging systems (Chu et al. 2015; Gao et al. 2016; Nyein et al. 2016). Additionally, smart bandage systems, with printed Internet of Things (IoT) pH sensors, can help monitor the stage of healing of a wound remotely.

Several pH-sensible materials have been investigated to tackle the challenges of traditional glass electrode pH sensors which include the leakage of electrolyte and the restriction of the device miniaturization.

One of the more popular sensor architecture is the printed electrochemical pH sensors. Printed sensors can be fabricated by various printing techniques such as inkjet-, screen-printing, flexography, and aerosol-jet printing. There are many industries related to the environment, agricultural, food and medical domains that use these kinds of techniques for developing sensors. There are two important variables that the success of printed electronics technologies depends on them: suitable post-processing techniques and the availability of functional materials (Renedo, Alonso-Lomillo, and Martínez 2007; Simić et al. 2016).

.

1.1.1 Potentiometric pH Sensors

pH sensors are based on potentiometric, amperometric, chemiresistive, electrochemical, and optical methods (Lowe et al. 2017; Parrilla et al. 2019; Qin et al. 2015). Potentiometric printed pH sensors are one of the most popular as the size can be easily miniaturized to be embedded in flexible and stretchable devices. In contrast with glass electrodes, the device structure of solid-state potentiometric sensors is simple, and the fabrication process is cost-effective (Park et al. 2019a). The potentiometric pH sensor works on the basis of the generation of an electromotive force (EMF) difference between a pH-sensitive working electrode and a reference electrode. The electromotive force (EMF) in an electrochemical cell, which is made up of a working electrode and a reference electrode, is measured in a potentiometric measurement, in theory. Using the Nernst equation, the pH of the sample is determined by comparing the EMF values obtained in the sample (E_s) and a standard buffer solution (E_b) with a known pH (pH_b):

$$pH = pH_b + \frac{(E_b - E_S)F}{RT \ln 10} \tag{1.1}$$

where R is the gas constant, F is the Faraday constant and T is the temperature (Rérolle et al. 2012).

The reference electrode can be made from Ag/AgCl for its low environmental impact and excellent potential stability. The pH sensing materials typically involves conducting polymers and metal oxides (e.g., WO_3, RuO_2, TaO_2, and TiO_2) (Manjakkal, Djurdjic, et al. 2015; Zhao et al. 2010; Zhou et al. 2019). Among conducting polymers, polyaniline (PANI) and its different oxidation states are pH sensitive (Manjakkal, Dervin, and Dahiya 2020). The transformation of emeraldine salt (ES) and emeraldine base (EB) under acidic and alkaline solution exposure is reversible, making PANI ideal for pH sensing (Manjakkal, Dervin, et al. 2020). Based on this characteristic, PANI can be used, as the pH sensing component, to modify the working electrode for enhanced sensitivity. PANI is well dispersed in solvents such as n-methyl-2-pyrrolidone (NMP), making it suitable to be printed in a reproducible thin film.

Advances in fabricating reduced size and flexible pH sensors will lead to integration on curved surfaces and applications with limited volume, such as smart bandage systems (Park et al. 2019a). In this work, we combined the advantages of potentiometry and printing technology. Screen printing is one of the most industrial, scalable, and low-cost processes among printing methods while potentiometry has a fast response compared to other types of sensors such as chemiresistive sensors, which enable pH sensors to recognize dynamic changes of analytes (Lamas-Ardisana et al. 2017; Parrilla et al. 2019; Qin et al. 2015). Additionally, printed electronics techniques are gaining more attention recently for fabricating electrochemical and electronic devices, solar cells, sensors, and displays (Agarwala et al. 2017; Jović et al. 2018; Xu et al. 2018). Here, a robust, low-cost and fully screen-printed potentiometric pH sensor was fabricated by screen- printing on top flexible polyethylene terephthalate (PET) substrates. The sensor has a working electrode consisting of a PANI-ES/G printed film and an Ag/AgCl as the quasi-reference electrode. By measuring the EMF between the two electrodes, the pH sensor quantitatively gives the pH level according to the Nernstian equation (Mahinnezhad et al. 2021).

1.1.2 Electrochemical pH Sensors

Electrochemical sensors are most broadly chemical sensors in different sectors. The sensing materials as working electrodes work in host system without damaging the system. The electrochemical sensors transform the electrochemical reactions into a meaningful analytic signal. There are two main parts in an electrochemical sensor which a chemical (molecular) recognition system and a physicochemical transducer that performs as a working (or sensing) electrode, the two other electrodes (reference and counter electrodes) are used for electrical measurements. Voltammetry, potentiometry, amperometry or conductometry can be used to convert a chemical signal into an electrical signal (Bellew et al. 2014; Sharma et al. 2021).
In three-electrode system in electrochemistry, the reference electrode provides a stable potential, the working electrode is where the reaction occurs, and the counter electrode provides a path for the reaction to occur, which is a better way to characterize the WE and the sensing materials performance. A two-electrode system, on the other hand the potential is measured between the two electrodes, and a separate counter electrode is not needed. Three-electrode systems are preferred for precise measurements as they provide better control over the potential, while two-electrode systems are simpler and can be used in cases where a high level of accuracy is not required.
In my work, in order to investigate the printed RE and its challenges and the possibility of reaching a fully-printed potentiometric sensor I used the two-electrode system in which we do not have the CE and the voltage generated between WE and RE is what we measure which is one of the challenges in stability of the sensor and will be presented in next chapters.

Electrochemical pH sensors are on high demand in different applications and industries such as food packaging, Biomedical applications, health monitoring, agriculture, and water treatment systems etc. Due to their wide sensing range (2–12), fast response (<10 s), close to Nernstian response up to 59.12 mV/pH sensitivity, easy integration on flexible substrates to use in wearable systems, low cost of fabrication and biocompatibility. This project represents an in-depth review of a range of polymers and MOx materials that have been used to fabricate pH sensors, based on different methods (e.g., conductimetric, potentiometric, chemiresistive,

extended-gate field effect transistor and ion sensitive field effect transistor (ISFET) and etc.). The techniques such as potentiometric and electrochemical impedance spectroscopy commonly utilize to describe these pH sensors. In the case of materials and the design of sensors for different applications, the main challenges are the interference of ions or other analytes, the potential toxicity of materials, the flexibility and cost of materials. In this part, the examples of some of the designs of pH sensors and their applications in flexible and wearable biosensors and metal oxide-based and also polymer based composite sensing material which can be used in medical applications and have been examined to present their suitability to be used in futuristic applications have been reviewed. Furthermore, electrochemical sensing process is surprisingly selective and such devices provide repeatable, accurate and quantitative results with low-cost measurement equipment. By combining each of different printing techniques and various materials and continuing to innovate, the production of flexible and low-cost electrochemical sensors is certainly within reach (Chen and Chatterjee 2013; Manjakkal, Szwagierczak, and Dahiya 2020).

There is a growing need for portable, rugged, sensitive and economical pH sensors for use in many areas such as the food industry, agriculture, medical organizations and oil refineries (Kahlert 2008; Lafitte et al. 2008). Traditionally the glass electrodes which work on the basis of potentiometry, has been used for pH sensing but they have disadvantages such as requiring frequent re-calibration and instability and/or drift (Wildgoose et al. 2003). Pioneering work by Hickman et al. demonstrated that designing a calibration-less system which works on the basis of measurement of the potential difference between a pH sensitive redox compound and a second pH insensitive redox compound can solve this issue (Hickman et al. 1991). This approach is developing more as it can replace the conventional glass electrodes which are expensive, fragile and it is difficult to implement them in flexible systems such as many wearable devices (Naumann et al. 2002).

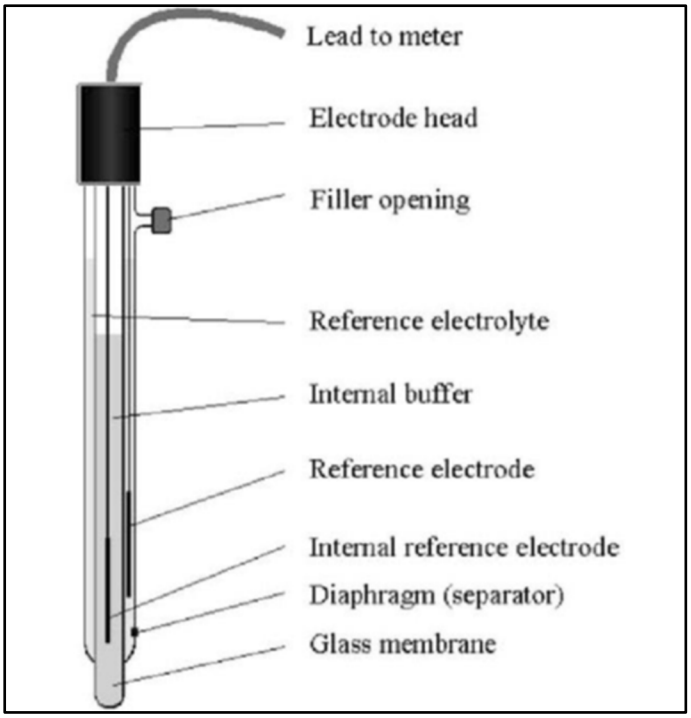

Figure 1.1.1 Schematic construction plan of a pH sensor (Naumann et al. 2002)

However, there are limitations in pH sensing range which is depend on the pKa of the chosen pH sensitive redox compound for example, when using anthraquinone as the active compound the sensing range of pH is over 4 to 10. 5 Carbon materials are extensively used in sensing layers in many electrochemical sensors. Particularly, in pH sensing applications different types of carbon materials have been used as they are low cost and due to their good electrical conductivity, availability and suitability for functionalization. There are a range of diverse strategies to functionalize carbon materials with pH sensing compounds, such as covalent bonding of target pH sensitive compounds by using chemical or electrochemical activation, also physical adsorption and co-polymers which can be molecularly attached to nanomaterials such as carbon black and carbon nanotubes (Kahlert 2008; Leventis et al. 2004; Wildgoose et al. 2006). In this field there are a range of various materials which are being explored via immobilization onto suitable substrates and working electrodes such as carbon electrodes (Lawrence et al. 2007). In some cases, films of the pure pH sensing materials are preferred. Lawrence et al. demonstrated that such immobilization strategies can be utilized to

functionalize pH sensing materials but need to be developed in order to readily be implemented in commercial pH sensors because in some of these modified layers on electrode substrates are unstable and instances, for example, in some conditions such as when solution flows across the electrode surface can be normally encountered (Kadara, Jenkinson, and Banks 2009). On the other hand, the concept of developing these kinds of sensors on a large scale for commercialization needs to be addressed. In order to solve these two problems, epoxy electrodes have been reported (Kadara et al. 2008).

Electrochemical platforms can be fabricated by different printing techniques such as pad printing, air bushing, direct pen and screen printing, gravure printing and inkjet printing (Bariya et al. 2018; Hart, Turner, and Hopcroft 1996; Walker et al. 2008).
Electrochemical platforms can be fabricated by different printing techniques such as pad printing, air bushing, direct pen and screen printing, gravure printing and inkjet printing (Bariya et al. 2018; Hart, Turner, and Hopcroft 1996; Walker et al. 2008).

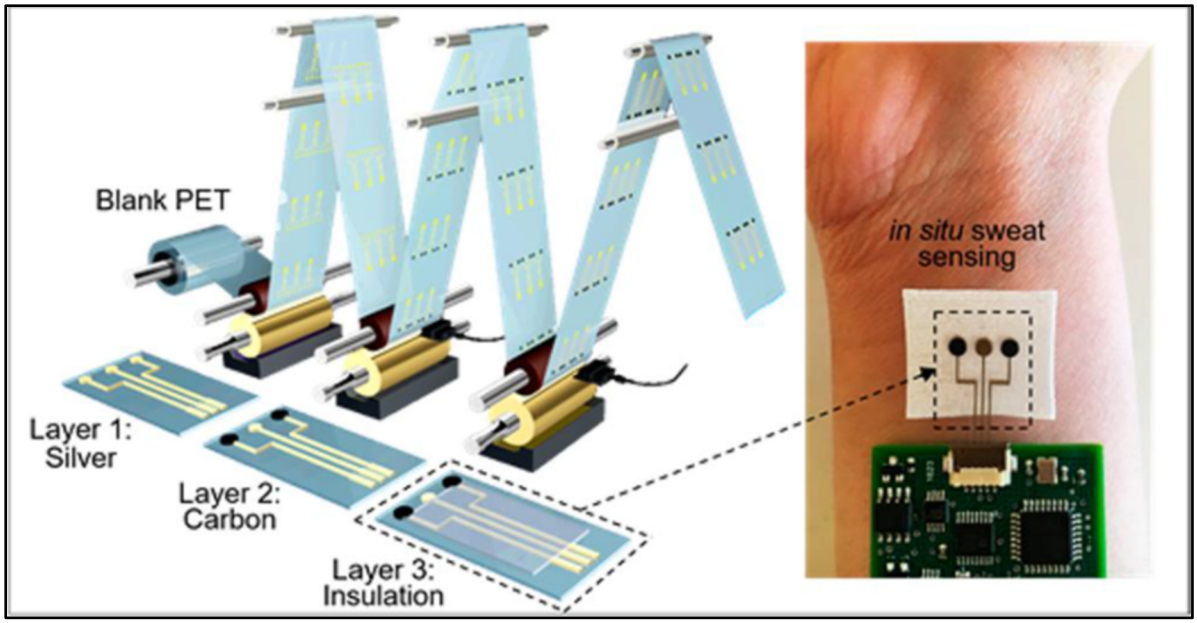

Figure 1.2 Roll-to-Roll gravure printing of biocompatible arrays of electrode on a flexible PET substrate allows low cost and high throughput production of the sensing electrodes that can be fabricated as density and size are controllable (Hart et al. 1996)

In Figure 1.2, Roll-to-Roll (R2R) gravure printed electrodes that can be fabricated in industrial amount and they have been utilized in a big range of electrochemical sensing applications have been demonstrated. It has been shown that these electrodes can be used as high-performance sensors to detect ions, metabolites, heavy metals, and some other small molecules in bio fluids by proper functionalization. This development of powerful and versatile printed electrodes using the R2R gravure represents a major translation step in the ability to build large-scale, low-cost disposable wearable sensors for health monitoring personalization programs (Hart et al. 1996). Screen printing has been developed over many years as one of the most industrial techniques to produce electrochemical sensors and one of its best known applications is production of disposable and low cost glucose sensors for diabetics to monitor blood glucose levels which has been demonstrated in Figure 1.3 (Da Costa et al. 2015; Tortorich, Song, and Choi 2013).

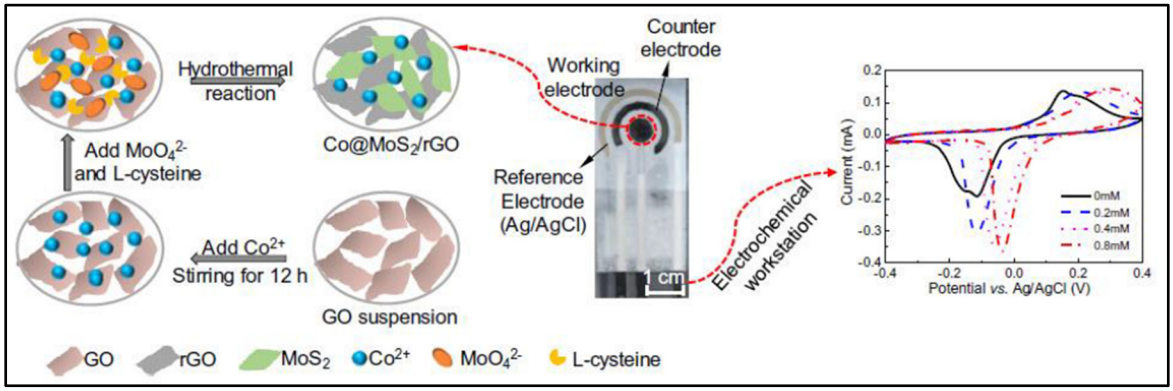

Figure 1.3 Schematic illustration of the fabrication of a screen-printed glucose biosensor (Manjakkal, Cvejin, Kulawik, et al. 2015)

Inkjet printing is another very well-known deposition technique as it is prevalence in office and home environments easily across the world. As a result of its popularity, inkjet printing is another low-cost technique with custom ink that can be utilized in paper-based and other flexible substrate electrochemical sensor fabrication (Li et al. 2020; Määttänen et al. 2013). On the other hand, sophisticated material printers are when greater precision and control are required as they allow for precise adjustment of ejection speed, ink droplet volume, and spacing. Additionally, nowadays there are a lot of high-end printers which come with heated beds which allow better control on the ink dry times when patterning the electrodes on a paper substrate. Figure 1.4 demonstrated an electrochemical sensor which a AgCl layer was

electrochemically deposited on silver strips to achieve a Ag/AgCl reference electrode. Lastly, a reaction well was formed on the paper platform using PDMS. Different electrode modifications have been performed on the sensor in this report such as electro polymerization of a polyaniline film on the surface of the working electrode using cyclic voltammetry in order to develop a potentiometric pH sensor.

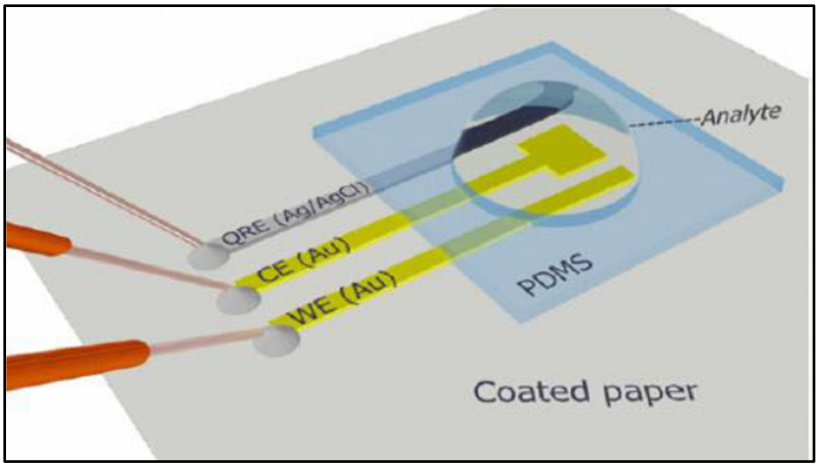

Figure 1.4 The illustration of an inkjet-printed electrochemical sensor on a paper substrate (Robinson and Lawrence 2006)

Furthermore, a glucose biosensor was fabricated by doing modification on the electrode surface using glucose oxidase (Manjakkal, Cvejin, Kulawik, et al. 2015). There is still a clear lack of knowledge in potential fabrication strategies and there are lots of research are going on to develop new types of pH sensitive and pH insensitive components which can be incorporated into other sensing applications. For example, an anthracene-ferrocene moiety has been introduced which is useful for fabrication of calibration-less sensing pH sensor but can also be simultaneously utilized in oxygen sensing devices as well as a pH sensor and also this sensor can function as a sulfide sensor (Manjakkal, Djurdjic, et al. 2015). There is still a lack of knowledge in using screen printing as the fabrication method in this field which can be beneficiary to those who wish to explore and develop as a large number of testing can be done on these sensors in academic environmental easily. A capacitive or conducti metric pH sensor works on the basis of the changes in electrical properties such as impedance or capacitance of a film deposited on interdigitated electrodes (IDE) when exposing to the electrochemical reaction occurring at the solution (Elnaggar et al. 2017; Manjakkal, Cvejin, et al. 2016).

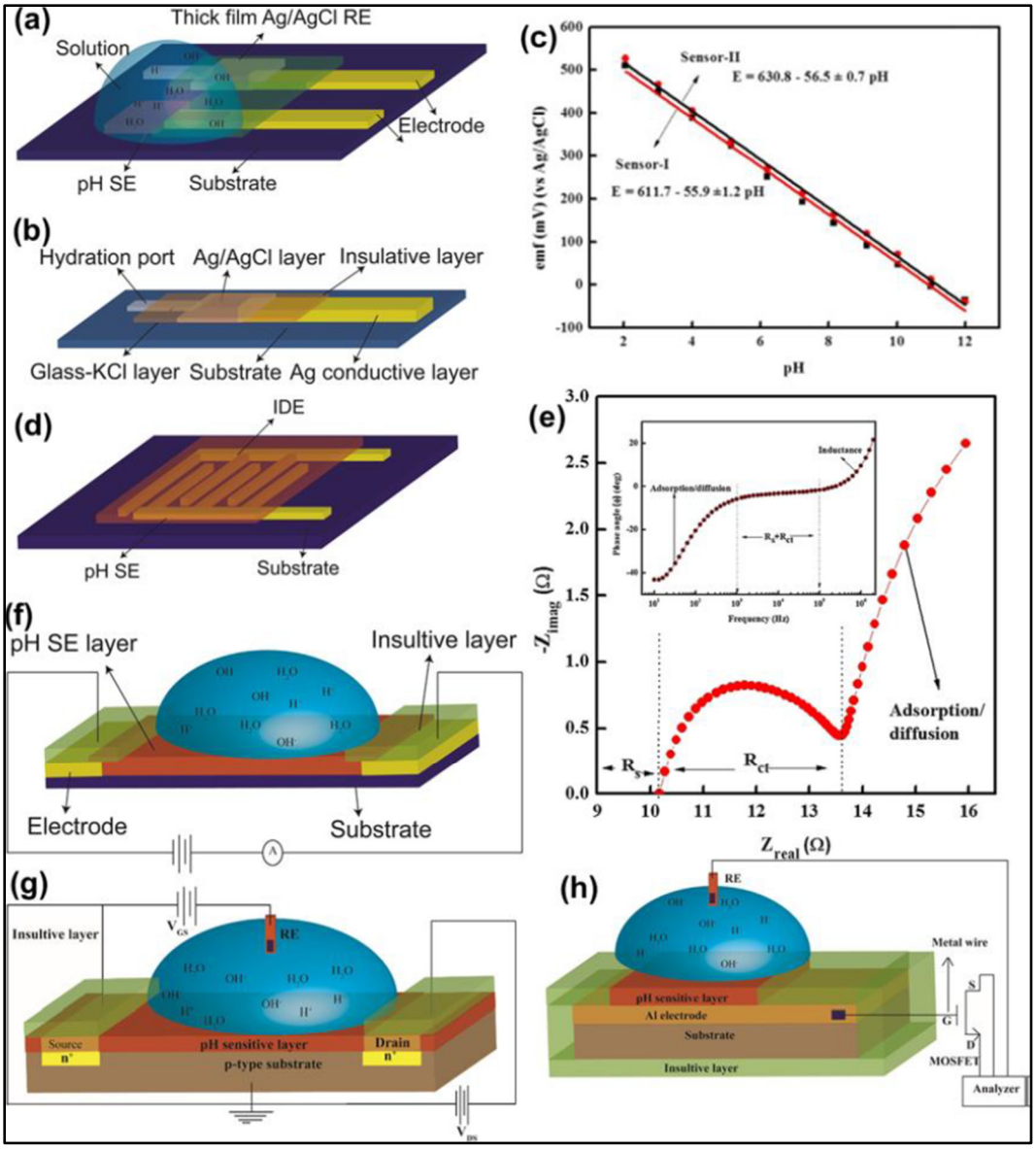

Figure 1.5 (a) Schematic representation of potentiometric pH sensor. (b) Schematic representation of thick film Ag/AgCl RE (c) Nernstian response of RuO2 based pH sensor, (d) Schematic representation of IDE based conductimetric pH sensor, (e) EIS analysis representing the Nyquist plot and Bode plot (inset) of RuO2 based thick film pH sensor for ion exchange and charge transfer. Schematic representation of a (f) Chemiresistor (g) ISFET and (h) EGFET (with measurement setup) based pH sensors respectively (Manjakkal et al. 2014; Manjakkal, Cvejin, et al. 2016)

The majority of these conductimetric pH sensors operate without RE with the IDE structure (Gill et al. 2008; Manjakkal, Djurdjic, et al. 2015). As presented in Figure 1.5 ,an IDE-based

sensor is a simple two-electrode configuration of an electrochemical cell and is widely used for small applications of sensors, converters and (Korostynska et al. 2007; Manjakkal, Cvejin, Bajac, et al. 2015). The conductimetric method is one of the well-known methods as it is easier and less expensive than other techniques. As shown in Figure 1.5 (d), the fabrication of conductimetric/capacitive pH sensors is more simple and cheaper compare to other methods as it involves two basic steps which are deposition of IDE on a substrate and deposition of the sensing layer. Screen printing is one of the widely used deposition techniques for printing the conducting electrode and the sensing layer on a flexible substrate (Kumar, Kumar, and Aniley 2021; Manjakkal, Cvejin, Bajac, et al. 2015; Manjakkal, Synkiewicz, et al. 2016). The IDE-based structure enables mass production of sensors with reduced size, well-defined geometry, compression and sensitivity. Even though this type of sensor has several advantages, its applications are limited due to the possible damage due to long-term work in various biological and chemical conditions. In addition, the conductivity of the solution can have a significant influence on the performance of the MOx based conductimetric sensors in terms of sensitivity (Lasia 2002; Lvovich 2012).

1.1.2.1 Sensing Materials

Polymer based conductimetric sensors have been utilized in many biomedical applications. The electrochemical reaction at MOx- solution interface of an IDE based pH sensors can be investigated by using Electrochemical Impedance Spectroscopy (EIS) analysis. The EIS analysis is a non-destructive and steady-state technique which can be used for analyzing a complex electrochemical system in a large range of frequencies for sensors, super capacitors and batteries. This method makes it possible to measure the response of a circuit or an electrochemical system and is useful in elucidating the pH measurement mechanism of a MO_x sensor by receiving information about phenomena such as absorption, ion exchange, charge transfer, diffusion, etc (Manjakkal, Szwagierczak, et al. 2020; Xu and Zhang 2010). In Figure 1.6, potentiometric pH sensitivity of different metal oxide materials have been compared.

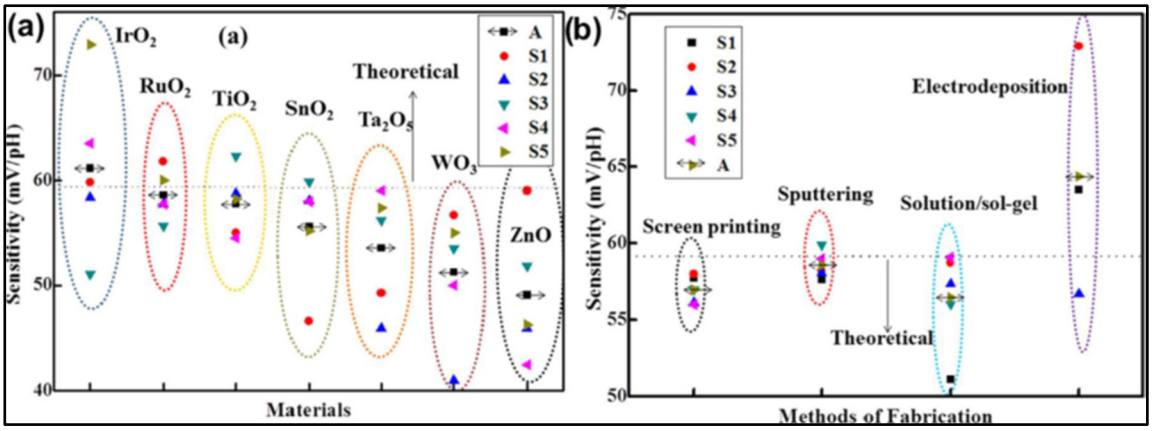

Figure 1.6 Comparison of potentiometric pH sensitivity of different metal oxide materials fabricated using different methods and the comparison based on the theoretical slope of Nernst relationship - variation of sensitivity with (a) materials and (b) methods of fabrication (A- average sensitivity, S1-sample #1, S2 sample #2, S3 sample #3, S4- ample #4 and S5-sample #5) (Yang et al. 2016)

1.2 Characteristics of electrochemical pH sensor

1.2.1 Response time

The time which is required for a solid state potentiometric sensor's open circuit potential (ocp) or electromotive force (emf) to reach 90% of an equilibrium value after immersing the sensor in a solution of a given pH value is the response time (Manjakkal, Zaraska, et al. 2016). The way to analyze the response time of a sensor, is to change the pH value drastically from the acidic to the basic solution and vice versa, and measuring the output potential. The response time of a metal oxide based pH sensor depends on many factors such as, the composition, structural properties, morphology, thickness, and pore size which are related to the sensing electrode. The response time of the sensor also depends on the range of pH value we are measuring. Most of the sensors have a faster response time when testing in the acidic region as compared to alkaline solution. For example, potential–time curves of IrO_2-rGO based sensor in buffer solutions with different pH value which are shown in Figure 1.7 (a) (Xu and Zhang 2010), demonstrates that at an acidic pH of 4, the sensor shows faster response time (150 s) than the sensor in a basic solution of pH value 12 (200 s). In almost all cases, the response time

of the sensor in neutral pH region is much slower in comparison to the both the acidic and basic regions (Xu and Zhang 2010). In terms of the comparison of the acidic and basic solutions, the fastest response of the sensor in acidic solutions is because of the ion exchange of small mobile H^+ ions, dominant in acidic solutions. In sensor based on RuO_2-Ta_2O_5 also have observed that in the acidic region of solution, the sensor exhibits a much shorter response time (< 8 s), than in basic solutions (< 15 s). This faster response is also related to the H^+ diffusion which effect is dominant in acidic solutions (Buck and Lindner 1994). The method of fabrication is another effective parameter on response time as it changes the morphologies and surface properties of materials, which are effective factors on the response time of pH sensors. As an example, Zhuiykov et al. (McMurray, Douglas, and Abbot 1995) showed that, for planar thick film Cu_2O doped RuO_2 sensing electrodes (SEs), the response time to pH changes was depend on the electrode thickness and it was decreasing from ~80 to 120 s for a SE thickness of ~2 μm to ~25 s for a thickness of ~5 μm (McMurray et al. 1995). These kind of changes in response time are because of the surface electrochemical reaction associated with the grain size and grain faceting of the SE and its inner active surfaces (shown in Figure 1.7 (b)). With increasing the thickness of the film the porosity increases and when a solution reacts on the surface of the MO_X layer in SE, three complex interfaces can be observed (i) outer surface: The metal oxide SE/solution macro-boundaries (ii) inner surface: The metal oxide SE/solution micro-boundaries because of the penetration of the ions in the liquid in inter-grain regions and pores (iii) The metal oxide SE layer/supported by Pt layer interface. In order to achieve a faster response in the sensor, the first two interfaces are very important to be considered. The ions from the outer active surface can be diffused or adsorbed into the inner active surfaces. Crystalline properties of thin and thick film SE can be compared in terms of their effect on the response time. The thicker film increases the porosity and larger grain size (1.5–2 μm) as well in compare to the thin film (grain size 600 to 800 nm). The inner active region's dimension of the thick film would be in the range of 50–110 nm. For this kind of SE, the thicker film can result in the faster response due to the well crystallized material.

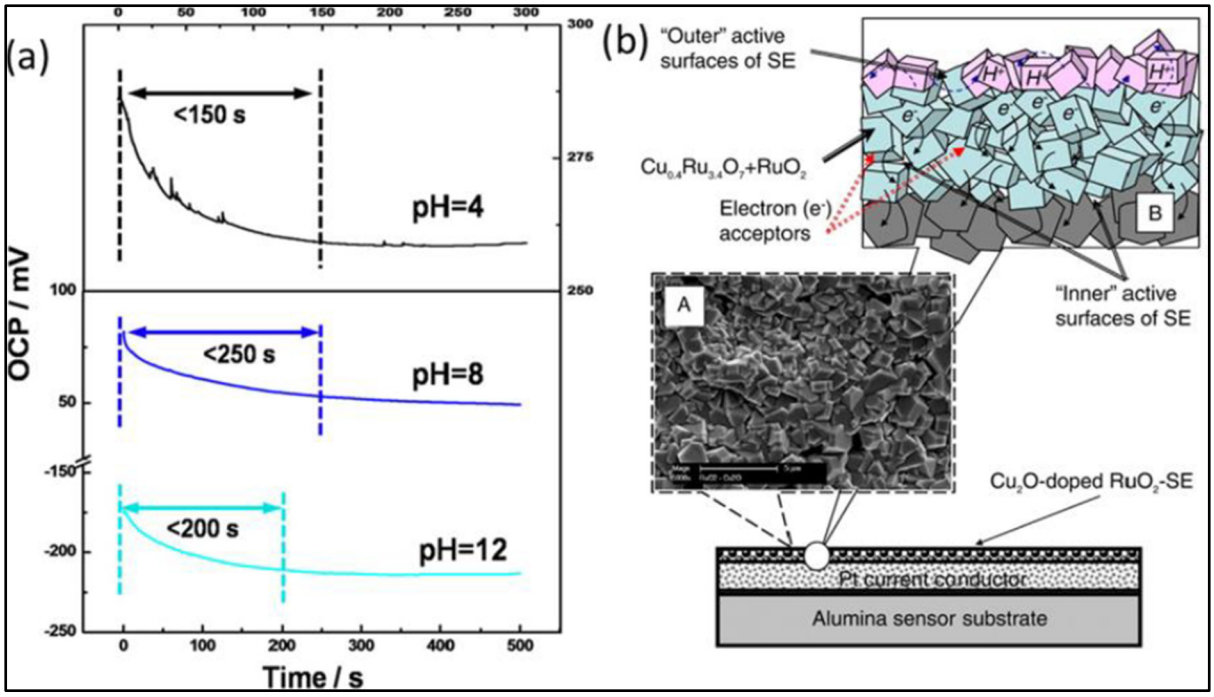

Figure 1.7 a) The response time curves of a IrO2-rGO based sensor in buffer solution at different pH value. b) A cross-sectional view of the Cu2O doped RuO2 SE on substrate (A) SEM image of surface of SE (B) tortuous paths of charge carriers to the Pt current conductor (Buck and Lindner 1994)

Similarly, Xu and Zhang (Buck and Lindner 1994) showed that the response time is less than 40 s for the sensing electrodes based on RuO_2 nanoparticles which were modified by vertically aligned carbon nanotubes (RuO_2/MWCNT) deposited by magnetron sputtering (Buck and Lindner 1994). Both, the porosity of the sensing film and also the nanostructured nature of it may improve the response time. With SEs based on RuO_2 with using glass addition (mainly commercial pastes), a slower response in basic solutions was noticeable as well. This could be due to the partial leaching of the glass which was present as the component in the sensitive layer. It was also observed that the response time of a pH sensor made of RuO_2 commercial paste is much better and higher. Higher glass compound in the commercial paste would lead to smaller open porosity and better compactness in the sensing layer. This would reduce the diffusion rate of protons in the RuO_2-glass layer and would lead to an increase in response time (Buck and Lindner 1994).

1.2.2 Interference effect and selectivity

One of the major disadvantages of a metal oxide pH sensor is interference of other ions on the sensing performance in the WE. Several reactions can be occurring due to the presence of different ions in both the acidic and basic pH ranges solutions and this effect the potential of the sensor when measuring. The selectivity coefficient of an ion depend on the SE characterizes give the ability to distinguish a particular ion from others.

According to International Union of Pure and Applied Chemistry (IUPAC) recommendation, the selectivity coefficient, KA, B can be is evaluated by means of measuring the EMF response of ion-sensitive electrodes immersed in mixed solutions of primary ion, A, and a less desirable or interfering ion, B (Fixed Interference Method, FIM) and also in separate solutions of A and B (Separate Solution Method, SSM) (Patolsky and Lieber 2005). The interfering effect of common anions (Cl^{-}, Br^{-}, $SO4^{2-}$) and cations (Li^{+}, Na^{+}, K^{+}, Ca^{2+}) is usually insignificant in majority of metal oxide based pH sensors [64]. However, the literature shows that the SEs made of commercial pastes show susceptibility to interferences caused by common anions such as halide, sulphate, carbonate ions because of the presence of lead in the SE (Mulchandani and Myung 2011). The influence of the ions in sensor performance depends on the type of materials and concentration of ions in the solution.

There is an increasing demand for reliable sensors to be utilized in online monitoring applications. Research on fabrication of metal oxides MO_x based pH sensors are increasing in academic environment. Such sensors, including those fabricated using thick and thin film methods, have been gaining significant attractiveness in current fabrication of electrochemical sensors' technology. This project presented an overview of the measurement techniques, fabrication methods and the sensing performances of widely used metal oxide-based pH sensors. Major techniques which can be employed to provide the information about the sensing mechanism of these pH sensors were also reviewed. With production of wide pH sensing range, fast responses, excellent sensitivity, the ability to be integrated with microelectronic components, wearable structural compatibility, biocompatibility, ability to integrate with

paper, clothes, skin, etc., the metal oxide-based pH sensors have a lot of advantages over glass based sensors.

1.2.3 Chemiresistive pH Sensors

The ability to change conductivity by a few orders of magnitude when pH change can develop a conductometric or chemiresistive type pH sensors.
Chemiresistive sensors have the advantage of simple structure and being easy to miniaturized which brings the ability to be implemented in various devices and high throughput sensor arrays. They also have the disadvantage of longer response time in compare to electrochemical sensors.

One of the most well-suited materials as chemiresistive sensors are polyaniline-based nanocomposites as their one-dimensional nanostructure lead to large conductance change as pH change their large surface area-to-volume ratio results in high sensitivity (Kishore et al. 2022).
The sensing mechanism of the chemiresistive sensors based on nanocomposites shown in Figure 1.8 as well as a photograph of a fabricated NIT.

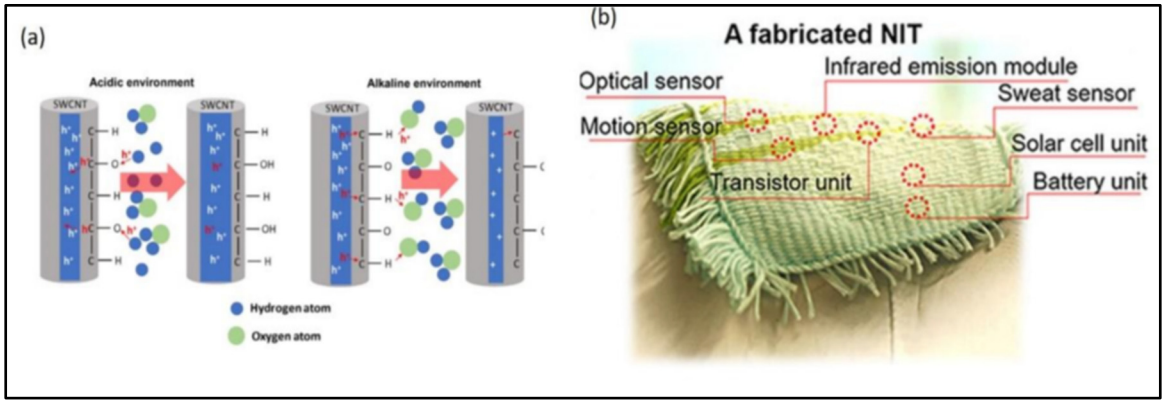

Figure 1.8 (a) Sensing mechanism of the chemiresistive pH sensors based on nanocomposites . (b) Photograph of a fabricated NIT with a typical NIT-type IC (Yang et al. 2021)

1.3 Printed Electronics Technologies

For many years, mercury was the most suitable material as electrode due to its highly reproducible, renewable and smooth surface. Various non-mercury electrodes have also been examined, with the advancements in electro-analytical science such as, bismuth and carbon electrodes. The construction of printing devices on flexible substrates has made it possible to develop a wide range of new electrode systems (Matthews et al. 1987).

1.3.1 Review

Traditional printing techniques are classified into impact and non-impact printing. In impact printing, the design on the substrate is created by partial Ink transfer through carrying information medium, printing page (a fixed image carrier). On the other hand, non-impact printing techniques are based on digital information control (Design or image) and do not need any stable means of information transfer such as printing Plate. Printed electronics uses traditional additive processes such as screen, flexography, aerosol, ink-jet, etc. for the fabrication of electronic systems such as sensing devices. Printed electronics are ecofriendly, meaning many organic materials can be used with these fabrication techniques. They also require low energy in both the manufacturing process and in operation. The fully printed sensors on flexible substrates such as paper and plastic offer lightweight, mechanical flexibility and thinness (Carrilho et al. 2009). There is a huge potential market for PE that needs a lot of time and effort to develop. These market products can be classified into the following groups:

• Organic/inorganic photovoltaics

• Integrated smart systems (RFID, sports fitness/healthcare devices, smart cards, sensors, and smart textiles)

• Lighting (OLED)

• Electronics and components (memories, antennas, batteries, wiring and interconnects, and other components)

• Displays (front planes such as, for example, OLED, e-paper, and electrochromic and their active matrix back plane)

A wide range of printing methods have already been used in conventional electronics manufacturing. They include screen printing, inkjet printing, gravure printing, flexo printing and offset printing. They are also applicable to many advanced PE products. Depending on the nature of the PE products, the right choice should be made in terms of ink, substrate, designed device structure, pattern geometry, production speed, performance, quality and production price. The important printing parameters are as follows:

1. Print accuracy and resolution: The displays for smartphones and computers require a pattern resolution of more than 300 pixels per inch (ppi). A resolution of a few micrometers with a precision position of 5 micrometers will be required. Multi-layered printing accuracy is also an important factor.
2. Uniformity over a few centimeters to more than 1 square meter is required in combination with optimized ink compositions and drying processes.
3. Wetting control and interface formation: Smoothness of a few nanometers to a few tens of nanometers are required for many OLED applications such as TV and lighting because the thickness of a typical OLED layer is less than 100 nanometers. Clarity at the edges of the pattern and bonding with the substrates depends on the material of the substrate (acceptance layer) and its design.
4. Compatibility of inks with printed parts such as rollers, masks, blades and inks have a significant effect on the performance and quality of mass production.
5. Power and cost considerations: One of the major benefits of PE technology is its mass production at a reasonable cost. High speed and high-quality print patterns should be maintained for hundreds of prints (Suganuma 2014).

The screen printing process allows for various electronics to be printed with very little material wastage. the screen-printing (thick-film) technique can be widely used in high throughput fabrication of products such as biosensors, which are extremely flexible and low cost (Vidal, Garcia-Ruiz, and Castillo 2003). The possibility of fabrication and design the screen-printed electrodes, such as microelectrodes and also chemically modified ones and using them in a

variety of highly sensitive biosensors has increased interest of using this technique in clinical, industrial and environmental fields (Matthews et al. 1987).

1.3.2 Screen-printing

Screen printing is one of the most popular technologies in printing electronics because it has been long time that is common in the electronics industry to print metallic connections on circuit boards. It is faster and more versatile than other printing methods because it adds simplicity, cost-effectiveness, speed and compatibility to the production process. Screen printing results can be reproducible by repeating several steps, and optimization of the process is possible depend on the materials characteristics (Søndergaard, Hösel, and Krebs 2013; Tobjörk and Österbacka 2011). Screen-printed electrodes can be used in real life applications, with notable benefits. One of the most successful examples in this field is the glucose biosensor (Matthews et al. 1987). There are two different assemblies of screen printers, the flatbed and rotary which are used for roll-to-roll printing presented in (Figure 1.9) (Søndergaard et al. 2013).

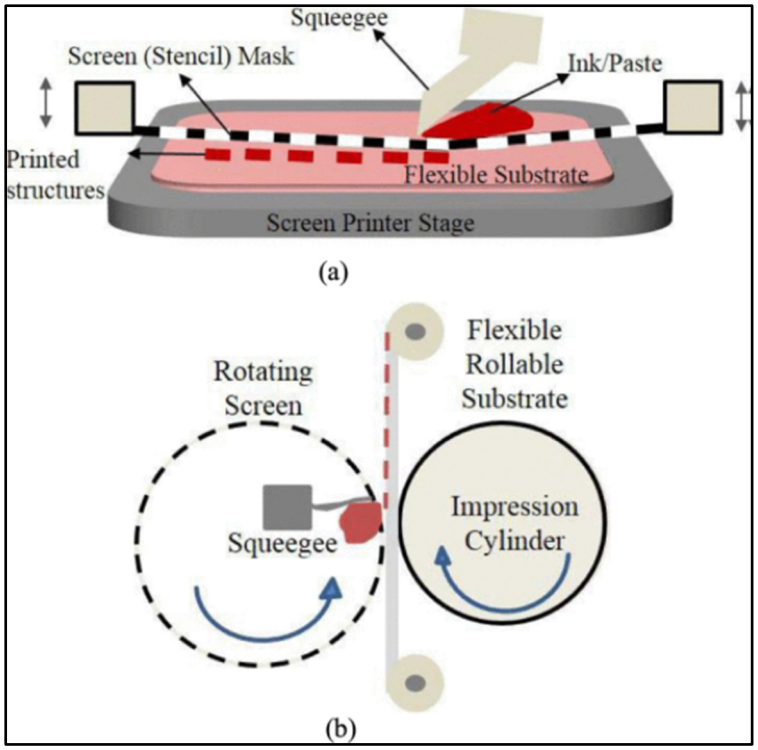

Figure 1.9 (a) Flatbed Screen printing (b) Rotary screen printing (Søndergaard et al. 2013)

Flatbed screen-printing is a useful method for small laboratory productions. High speeds in fabrication process can be achieved by using rotary screen printing, but the screens for this technique are expensive and difficult to clean (Søndergaard et al. 2013). Although screen printing is a simple technique, the printing quality and characteristics are affected by many factors such as ink viscosity, angle and geometry of the squeegee, snap off between screen and substrate, printing speed, mesh size and material (Jabbour, Radspinner, and Peyghambarian 2001; Søndergaard et al. 2013; Turunen et al. 2008).

The screen printer mainly consists of one or two squeegee and a screen with the desirable design on it. The printing process would be carried out by spreading the paste on the screen using the squeegee which is normally made of rubber. Porous fabric and stainless steel are the most known material for fabricating screen mesh. The design would be deposited on the screen

using UV light which allow the ink to pass through and create the electrodes on the substrate (Figure 1.10).

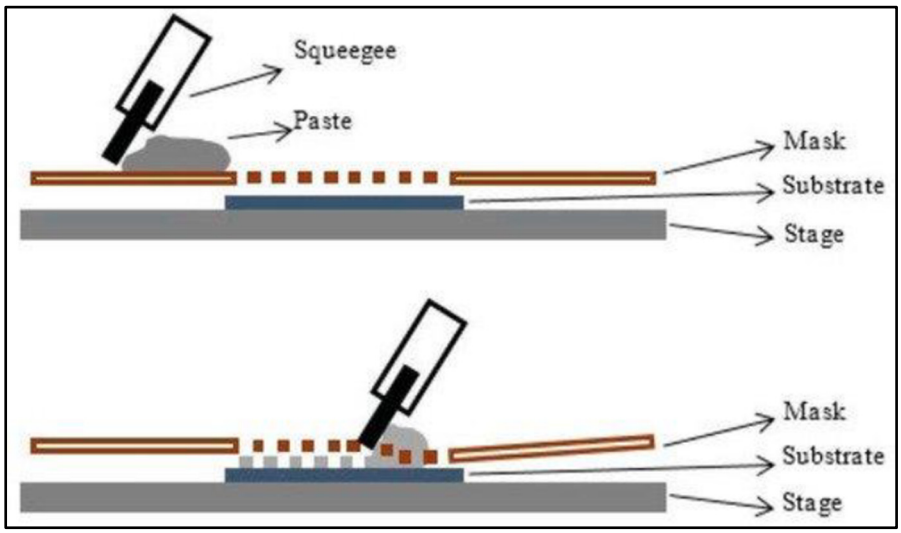

Figure 1.10 Schematic of screen printing process (Arrabito et al. 2020)

Screen-printing can be used to fabricate many kinds of industrial products as it is the fastest hand highest throughput technique in flexible electronics. A number of printed sensors, electronic devices and circuits has been fabricated by this method. For example, a TFT has been fabricated fully in screen printing which is shown and demonstrated in (Figure 1.11) (Cao et al. 2016; Khan, Lorenzelli, and Dahiya 2014). Also the first fabrication of OLEDs with screen printing has been demonstrated in (Figure 1.12), in this work effect of solution parameters i.e. viscosity of the solution and mesh count of the screen have been investigated (Jabbour et al. 2001; Khan et al. 2014).

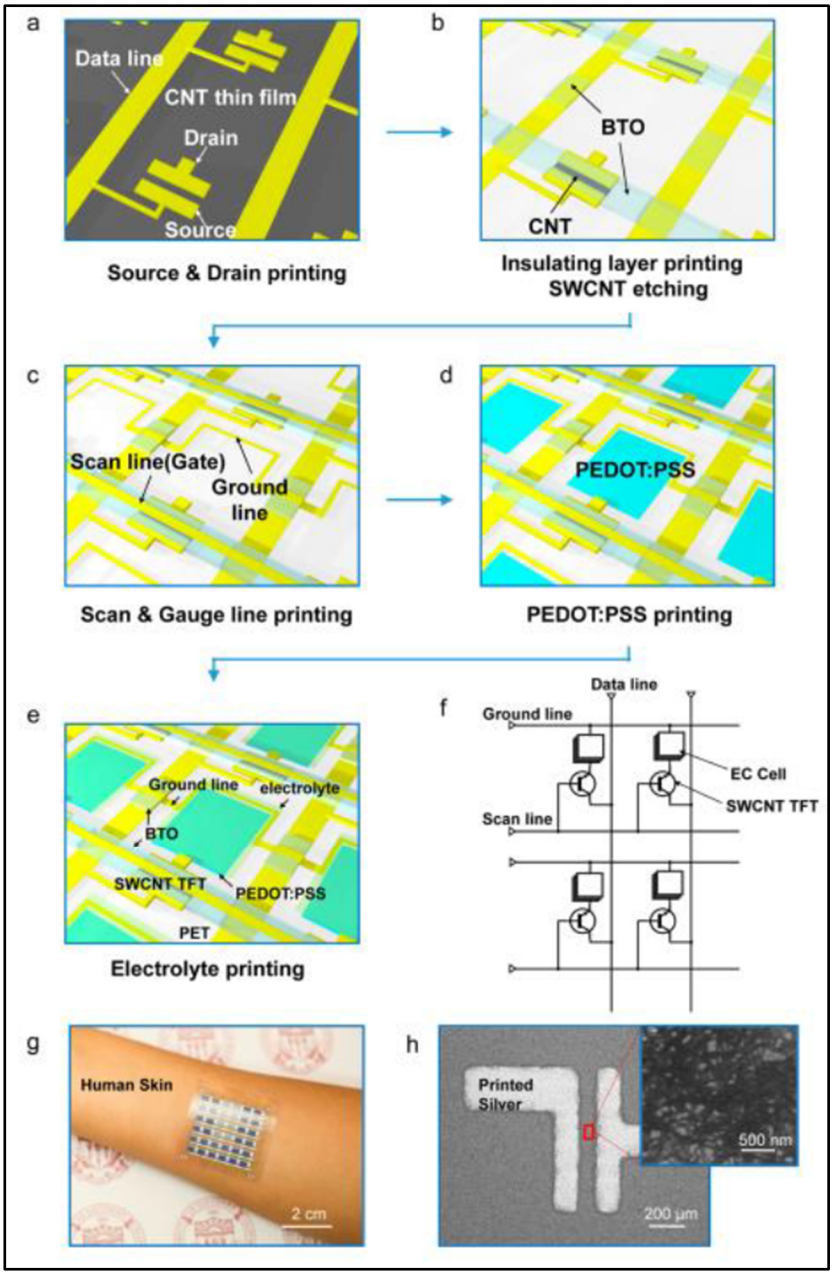

Figure 1.11 (a) 1. High-purity semiconducting SWCNTs were spin coated on a 5 × cm2 PET substrate to form a thin film. 2.The printing of source and drain electrodes and data lines in silver. 3.Printing a BTO layer on the channel region of each TFT. (b) 1. Printed BTO layer was used such as hard mask to etch and remove the unwanted SWCNTs outside the TFT region. 2.Then another BTO layer was printed as a passivation layer to protect the data lines and the ground lines. (c)-(e) Scan lines, ground lines, PEDOT: PSS layer, and electrolyte were screen-printed sequentially (Cao et al. 2016)

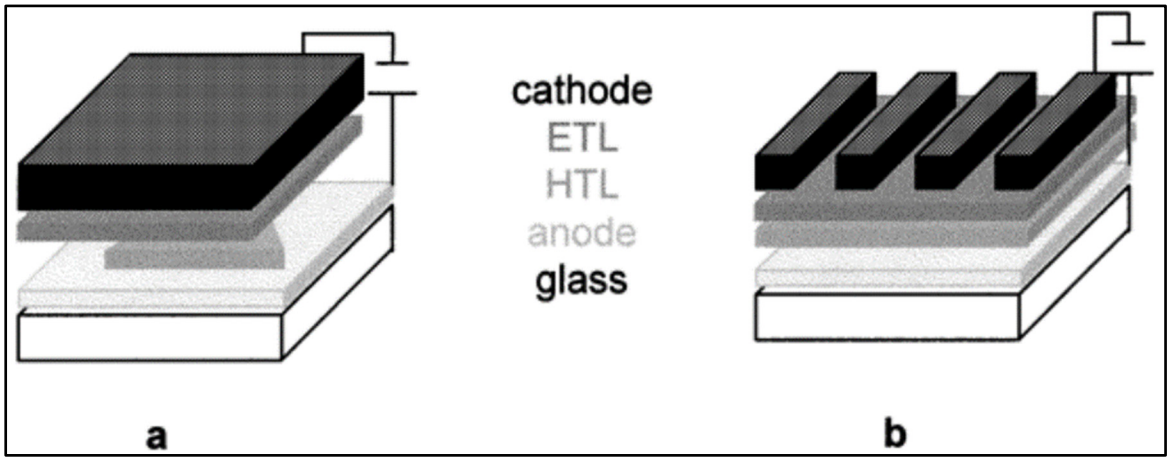

Figure 1.12 Structure of device with (a) patterned HTL and (b) patterned cathode (Vasilescu et al. 2016)

In screen-printing there is the possibility of printing several layers in different designs and materials to fabricate a complete device which gives us the ability to fabricate a variety of electrochemical sensors (Figure 1.13).

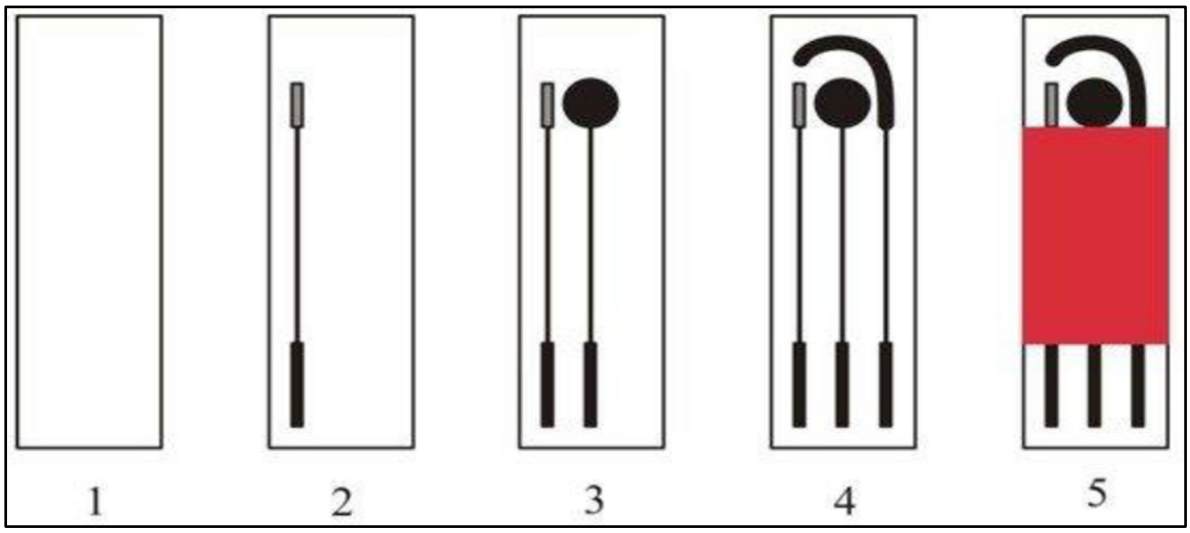

Figure 1.13 Fabrication of a three-electrode biosensor system on a chemically inert substrate (1). It involves of reference electrode (2), working electrode (3), and auxiliary electrode (4) Dielectric layer (5) (Vasilescu et al. 2016)

One of the new techniques for fabrication of screen-printed electrodes is the one-step deposition layer based on bio composite. In this technique all the materials, for example

graphite, catalysts, mediators, stabilizers, enzymes and polymers, can be mixed, forming a new formulation called bio composite ink or paste which have the characteristics to be screen-printed on to the substrate. This is one of the simplest configurations in producing biosensors which can lead to great rapidity and simple manufacturing process.

However, there are also the processes which requiring more complex optimization, because of the need to keep the initial properties and characteristics of materials while using them in different environment and conditions. Wang et al. (Wang, Pamidi, and Rogers 1998) have reported the development of an electrochemical immuno-sensor based on bio composite one-step strategy. One step-fabrication in this project involved using a sol–gel and screen-printing technology in which the printed ink was a dispersion of graphite powder, rabbit immunoglobulin G, and a binder. A year later the same group also reported the preparation of a highly sensitive ink used in a disposable glucose biosensor by dispersion of cupric hexacyanoferrate as electro catalyst and glucose oxidase as the enzyme in screen-printable carbon ink (Anon n.d.-b).

1.3.3 Aerosol-Jet Printer (AJP)

Aerosol-jet printing (AJP) is a newer printing technology which is a suitable tool to be used in academic research as it is more flexible in terms of physical properties of the materials that could be printed by this technique. AJP, is also considered as a highly effective method for printing nanoparticles inks in microscale dimensions. Studies have been done in order to optimize and analysis the properties of the inks can be printed by AJP and printing parameters (Secor, 2018). The printing mechanism of AJP is by atomization of the inks containing solvents and dispersed Nano particles and forwarding it to the medium surface by a carrier gas, deposited as the proposed design with great precision. AJP is a contactless technique which can print and observe the pattern simultaneously with it, it is easy to print the materials as the desired pattern, AJP has advantages over many traditional methods which make it suitable to be used in applied research fields such as transistor fabrication, complex circuits boards, and photovoltaic metallization.

In contrast, AJP has some disadvantages that are known to users. Even though a wide range of inks can be printed by this technique, adjusting optimal printing parameters is frequently a complicated process. Due this disadvantage, consistency and replication are challenging to achieve as frequent ink observation, replacement and optimization of printing parameters could be needed. Nuzzle blocking, and spattering ink over the substrate are the other challenges of using this method (Secor 2018).

1.4 Polyaniline based pH sensors

PANI is one of the pH–sensitive materials, owing to its strong which is widely used in various applications due to its pH sensitivity (Lindfors and Ivaska 2002), ionic and electron mixed conductivity (Bobacka et al. 1994), chemical stability and low cost (Geniès et al. 1990). In this work PANI has been used as the pH sensitive material. PANI can be synthesized by electrochemical polymerization on electrode substrates or the direct oxidation of aniline through chemical oxidants (Alam et al. 2018; Geniès et al. 1990; Karyakin et al. 1999; Wei et al. 2005). Direct electro-polymerization on electrode surfaces has advantages for the fabrication of miniaturized sensing chips. pH–response mechanism of PANI is based on PANI reversible protonation and deprotonation process. PANI has three oxidation states: fully reduced leucoemeraldine base (LEB), half–oxidized emeraldine base (EB) and fully oxidized pernigraniline base (PNB) (Geniès et al. 1990). Emeraldine base (EB), can be protonated and become the conductive form of emeraldine salt (ES) due to the presence of amine and imine groups. The reversible protonation and deprotonation of EB and ES form of PANI is the reason of pH–sensitivity property (Anon n.d.-a; Bandodkar et al. 2013; Lindfors and Ivaska 2002) (Figure 1.14). This is reversible reaction of transferring the protons and electrons, which is the base of the Nernstian response for PANI–based potentiometric pH sensors (Karyakin et al. 1996, 1999).

PANI–based wearable pH sensors has been used in a wide range of flexible wearable devices. A tattoo–based pH sensor fabricated with PANI was attached to human skin through screen-printing technology (Bandodkar et al. 2013). In that work, PANI film was obtained by electro–

polymerization with 25 cycles in aniline/HCl solution (Figure 1.15 (a)) and the potential response of the tattoo sensor after extreme deformation has been examined (Figure 1.15 (b)). Surprisingly, after bending 50 times and stretching 40 times the sensitivity of prepared tattoo sensor was increased from 52.8 to 57.5 mV/pH at a pH range of 3–7. This improvement in sensitivity was explained to be due to reorientation of the amorphous and crystalline phases of PANI. The tattoo sensor was successfully implemented for evaluating the pH sweat on neck, wrist and lower back. Recently, Cheng and coworkers fabricated a highly stretchable nanofiber pH sensor, prepared by the electrodeposition of PANI on gold fibers (Wang et al. 2020) (Figure 1.15 (c)). The prepared fiber–based pH sensors exhibited a high stretchability and a sensitivity of 60.6 mV /pH in a pH range of 4–8 under 100% strain. Lee et al. proposed paper–based PANI pH sensor that showed flexibility and biodegradable characteristics (Yoon et al. 2017) (Figure 1.15 (d)). The paper–based pH sensor exhibited a near-Nernstian sensitivity of (58 mV/pH in the pH range of 2–12) with a fast response time of (<10 s) and also good selectivity. The researchers above prove the flexibility and tensile properties of PANI, which make it to be deposited on various flexible substrates and to be implemented in wearable devices (Tang et al. 2022).

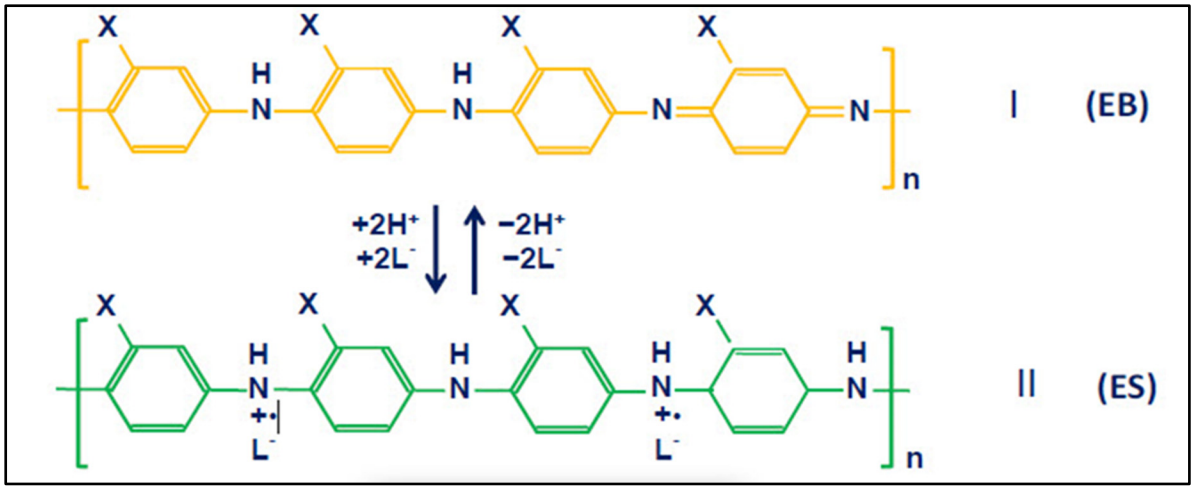

Figure 1.14 The mechanism of pH response for PANI and PANI derivates (X = H, CH3, C2H5 or C3H7) illustrating the protonation and deprotonation of the half–oxidized emeraldine–base (EB) and half-oxidized emeraldine salt (ES) forms (Lindfors and Ivaska 2002). Reprinted from, Copyright (2002) Elsevier

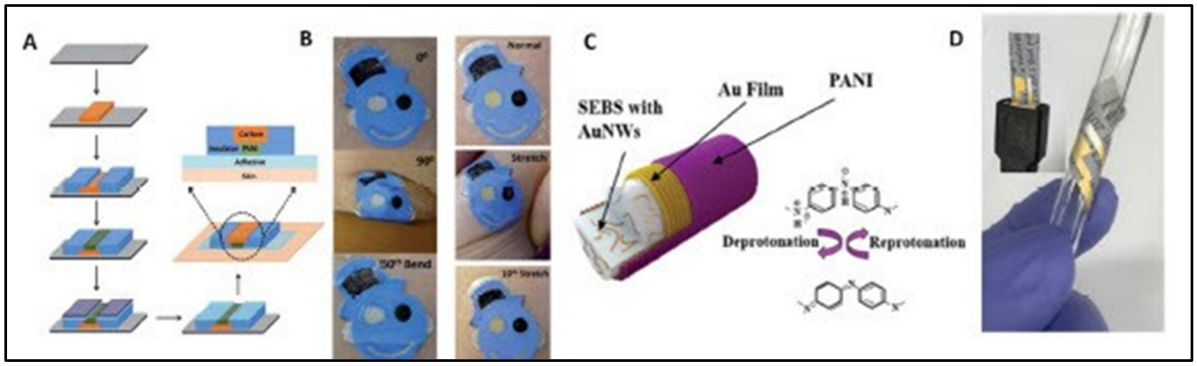

Figure 1.15 PANI–based wearable pH sensors. (a) The fabrication steps for PANI–based pH sensors on a tattoo substrate. (b) The tattoo applied to the cubital fossa at different bending and stretching states and cyclic tests. Reprinted with permission from (Bandodkar et al. 2013), Copyright (2013) Royal Society of Chemistry. (c) The structure of a fiber pH sensor deposited by PANI. Reprinted with permission from (Wang et al. 2020), Copyright (2020) Royal Society of Chemistry. (d) Paper–based pH sensor under bending tests. Reprinted with permission from (Yoon et al. 2017), Copyright (2017) Elsevier

CHAPTER 2

METHODOLOGY

At first, a fully screen-printed pH sensor based on polyaniline and graphite (PANI/G) nanocomposites has been fabricated and tested, then in order to investigate the effects of different ratios of polyaniline and graphite active nanocomposites on functionality of the sensors and to avoid viscosity limitations, aerosol-jet printing has been used along with screen printing to fabricate and test more sensors.

2.1 Materials and Apparatus

A. Reagents and solutions

The PANI-emeraldine salt (PANI-ES) powder (Mw >15,000), NMP solvent and buffer solutions were acquired from Sigma Aldrich. The Ag/AgCl paste was purchased from Sun Chemical. The commercial graphite paste and the dielectric passivation paste was bought from DuPont.

B. Apparatus

The pH values of buffered solution were adjusted by adding HCl or NaOH solution to standard buffer solutions (Cole Parmer). In order to control the accuracy of the measurements, the pH values were regularly validated by a commercial pH meter (Accumet AB 15/ 15+ bench-top meter). The potentiometry voltage-time (V-t) measurements were carried out with an Agilent 34401-A digital multimeter.

2.2 Preparation of the Active Nanocomposites

The sensing material was prepared by first dispersing 50 mg of PANI-ES salt powder (Mw >15,000) in 5 mL of NMP for 15 min using a 130 W sonication bath. The PANI solution was

subsequently added to 5 g of commercial carbon black paste and stirred for 30 min to homogenize the CB/PANI-ES paste mixture.

2.3 Screen Printing Parameters Optimization

The structure of the sensors and the electrodes can be designed using AutoCAD or other designing tools, after that we should develop a film using photo plotter machine and a development process which would be done in a dark room (Figure 2.1).

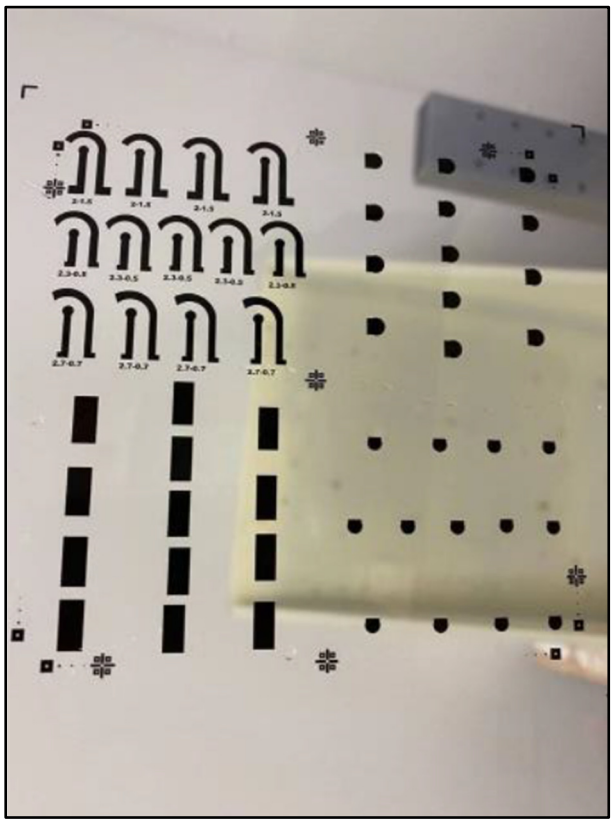

Figure 2.1 Photo plotter film

Then the pattern on the film would be transferred on the screen mesh which has been coated with an emulsion material by exposing under UV light then by developing with water the emulsion would be open as the desired design (Figure 2.2).

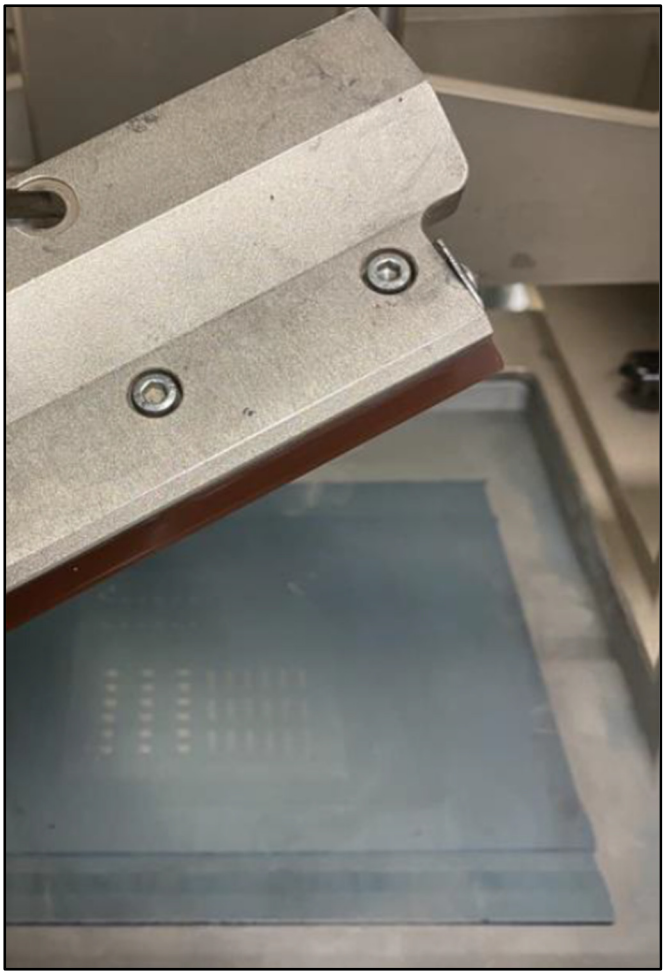

Figure 2.2 Developed mask (10 cm x 10 cm) and rubber squeegee

The paste viscosity and surface tension of the substrate are important factors which can determine if the paste can be deposit by screen printing or not. Screen printing technique is usually compatible with the high-viscosity pastes because low viscosity inks can simply run through the screen mesh and deposition of low viscosity inks to form the desired pattern is very difficult (Moonen, Yakimets, and Huskens 2012). The usual thickness of a screen-printed image is in the range of several tens of microns, but, especially when a thick screen is used, the thickness can exceed 100 micrometers with a single pass of the print, which is by no other technique is possible. For other Printing methods, such as inkjet or flexo printing, the usual thickness is less than 5 micrometers. Without considering the ink properties and mesh count

which are effective parameters on printed patterns' resolution and thickness, the common nominal values are 50-100 μ m resolutions and wet thicknesses is about 10-15 microns. As screen printing is a thick film technique it can enable us to print low-resistance structures, also with conducting polymers this can be possible to compensate the high-volume resistivity by printing a thicker layer (Shi et al. 2011).

The capillary number (Ca) represents the relationship between viscosity, surface tension and printing speed which are the most effective parameters in screen printing process and is defined as Ca= μU/γ, where γ is the ink's surface tension, μ is the ink's viscosity, and U is the printing speed which is typically around ~1 $mm \cdot s^{-1}$.

The screen printing process and parameters have been theoretically investigated by Kapur et al. (Siden and Nilsson 2007). In this work the importance of the surface effects has been studied when the liquid is pulled out from the mesh and is deposited on the substrate. They could confirm the validation of their model while using a wide range of model inks. They demonstrate that the common range of Ca for all the printers is in the order of 10, which is based on the typical viscosities about 10 Pa·s, also surface tension of 30 $mN \cdot m^{-1}$, and snap-off speed of 2 $mm \cdot s^{-1}$. For these reasons, actually screen printing process is generally independent of many of the experimental parameters, which makes this technique suitable for fabrication in large scale (Jabbour et al. 2001).

The printing speed and squeegee pressure on the screen surface while printing are two factors which can be optimized based on ink characteristics to improve the patterns' resolution, here is the investigation of these two parameters while printing a 100-micron width line through a stainless-steel mesh with 400 wire/inch which is shown in (Table 2.1).For the commercial carbon paste has been used in this project, increasing the squeegee pressure decreases printing resolution and quality (Figure 2.3-Figure 2.4) and with increasing the printing speed, the printing resolution decreased (Figure 2.5-Figure 2.6), these effects can be different while printing a low viscosity materials.

Table 2.1 Investigation of the effect of squeegee pressure on printing resolution while other parameters are constant.

Sample number	Curing Time	Curing temperature	Squeegee pressure	Printing speed
1	1 h	85 °C	0.1 MPa	90 mm/s
2	1 h	85 °C	0.12 MPa	90 mm/s

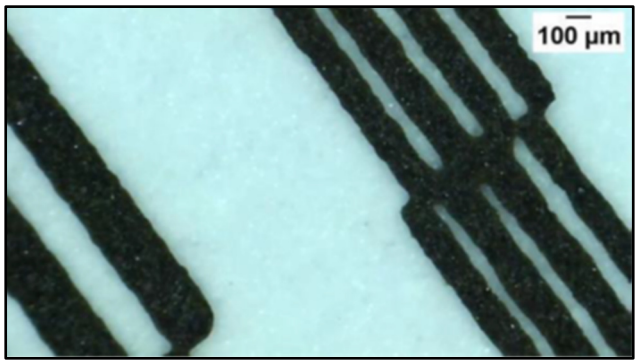

Figure 2.3 Squeegee pressure at 0.1 MPa

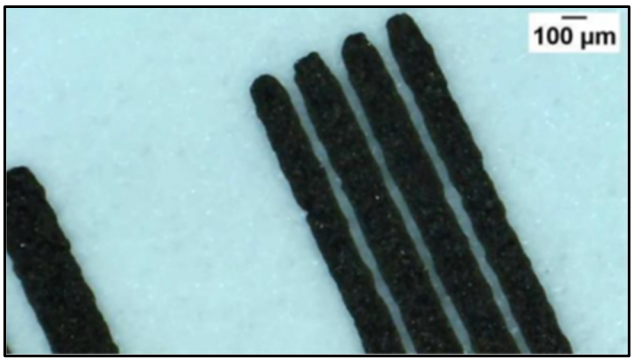

Figure 2.4 Squeegee pressure at 0.12 MPa

Table 2.2 Investigation of the effect of printing speed on printing resolution while other parameters are constant.

Sample number	Curing time	Curing temperature	Squeegee pressure	Printing speed
1	20 min	120 °C	0.15 MPa	110 mm/s
2	20 min	120 °C	0.15 MPa	80 mm/s

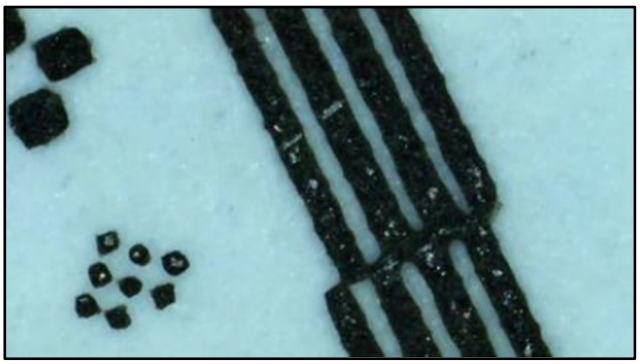

Figure 2.5 100-micron width line printed at 10 mm/s speed

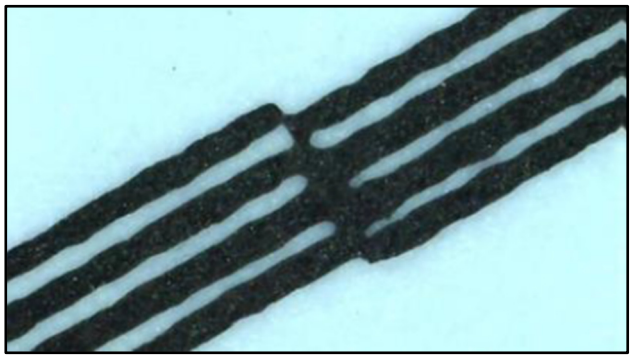

Figure 2.6 100-micron width line printed at 80 mm/s speed

Another important factor is the balance between surface energies of substrates and surface energies of the inks to obtain high-resolution structures (Cao et al. 2016; Wen et al. 2011). As surface energies of the substrates reduce the wettability of the solution would reduce as well, which improve the printing resolution and increase the chance of printing low viscosity inks. If the critical surface tension of the substrate would be lower than the surface energies of the inks, the printing quality and resolution would be good even with low viscosity inks. When using high viscosity inks, viscosity forces would result in high resolution. But when we need

to use low viscosity ink, wetting behavior is very important and would effect on the resolution. Although when using high viscous inks, the ink flow on substrate is minimize, but low viscosity inks are desirable as sometimes we need to print composites with low viscosities and also it can lead to dispensing the solution through the mesh and obtaining fine edges and better resolution. In this scenario, the wettability of the substrate should be controlled by adjusting the surface energies to be able to print the low viscosity inks. As the low viscosity inks have high degree of flow ability, this can reduce the possibility of mask blockage, and we would have better resolution and less surface roughness of the printing films (Khan 2016).

Material, the number of meshes in screen, layer of emulsion and screen strength are also play a major role in high-resolution patterning. The important factors of screen are the sizes of mesh openings and materials ranging from polyester to stainless steel is possible. The development in the screen mesh production technology has been made by modifying the strength with materials such as nylon, polyester and stainless steel. As strength and mesh count of the screen mesh increase leads to improving the printing quality. In large scale production using a screen mesh made of stainless steel with about three times more strength than conventional screen mesh is now possible (Khan et al. 2014; Vasilescu et al. 2016).

2.4 Fully Screen-printed Sensor Fabrication

The screen printing mask has been designed using AutoCAD and was developed to print all three layers aligned on top of each other (Figure 2.7).

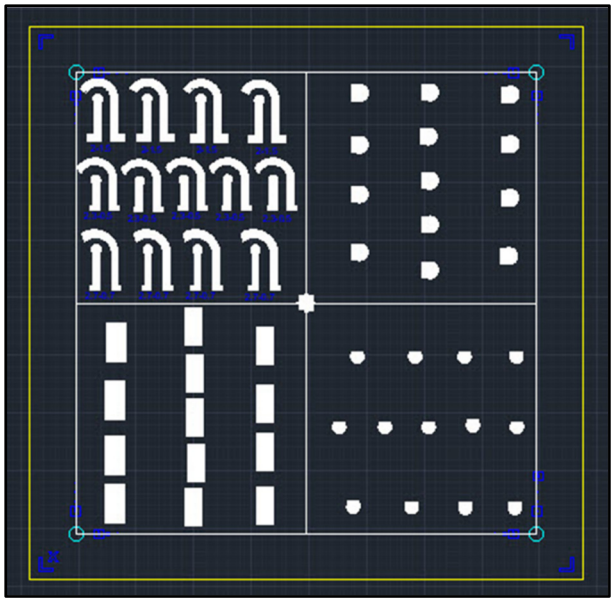

Figure 2.7 screen printing mask design

Reference electrode and the contacts were printed with Ag/AgCl paste as the first layer and dried in an oven at 120 ºC for 1 h. Then, the resulting paste was screen printed as the working electrode in a circular pattern over one of the Ag/AgCl electrodes and dried at 120 ºC for 1 h. The surface morphology of the active layer was studied using high resolution SEM (Hitachi SU-8230), and the thickness of Ag/AgCl electrodes and sensing layer was measured by profilometry (Bruker Dektak XT, USA). In Figure 2.8 (b), the cross-sectional SEM images showcasing the interface between carbon and Ag/AgCl indicate a strong adhesion between the two as there are no cracks or holes. Finally, the dielectric paste was printed on the electrodes to electrically isolate the contacts from the test solution and dried at 120 ºC for 1 h. The sensor dimensions were 13.5 mm length x 8 mm width x 20 µm thick, shown in Figure 2.8 (c).

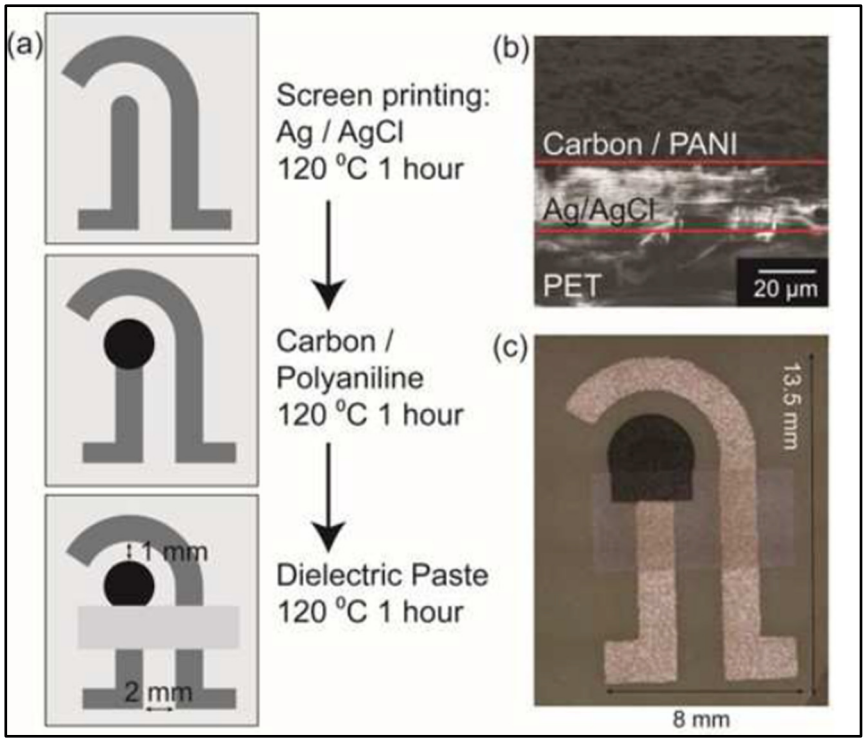

Figure 2.8 (a) Schematic illustration of the screen printing process of the different layers of pH sensors. (b) Cross-sectional SEM image and (c) top-view optical micrograph of the potentiometric pH sensor

The PANI-based working electrode is highly sensitive to hydronium $H3O^+$ ions, and the redox equilibrium between $H3O^+$ and PANI phase transitions is the working principle of the potentiometric pH sensor. Despite the stability advantages that the electrochemical polymerization of aniline on the working electrode surface brings, our nanostructured and porous CB/PANI-ES electrodes facilitate redox reactions [7]. Here, PANI-ES powder dispersed in NMP was used to modify the CB paste to be used as the pH sensing material. By doing so, this avoided the potentially toxic by-products from the polymerization process of PANI. Also, this CB/PANI-ES sensor is scalable and reproducible. In this work, various CB/PANI-ES pastes ratios have been tested to obtain the optimal sensor characteristics in terms of pH sensitivity, stability, and physical properties. The nanocomposites were prepared by gradually increasing the PANI solution ratio to control the viscosity of the graphite paste and

the composition of Graphite 99.1 wt% and PANI-ES 0.9 wt% could be printed easily with screen printing which also exhibited the highest sensitivity and stability for pH levels detection.

2.5 Preparation of the Active Nanocomposites with Significant Difference Between PANI and Graphite Ratios and Fabrication Process of the Sensors Modified with Aerosol-jet Printing

Active materials were prepared by a solution processing method with PANI-ES powder being dissolved in NMP solvent at a concentration of 10 mg/ml. The dispersion was stirred at room temperature for 20 min at 500 RPM. PANI/G composites were then prepared with different wt% of graphite by mixing graphite paste with PANI/NMP solution. The samples are listed in Table 2.2.3.

Table 2.3 The formulation of PANI/G composites at different weight percent of graphite.

Samples	Weigh percent of graphite content(wt%)
PANI-ES	0
Graphite	100
PANI/G 1	20
PANI/G 2	50
PANI/G 3	80

Sensors have been modified with three nanocomposites and sensors performance and materials properties has been characterized and compared.

2.6 Data Collection

The pH values of buffered solution were adjusted by adding HCl or NaOH solution to standard buffer solutions (Cole Parmer). In order to control the accuracy of the measurements, the pH values were regularly validated by a commercial pH meter (Accumet AB 15/ 15+ bench-top meter). The potentiometry voltage-time (V-t) measurements were carried out with the help of an Agilent 34401-A device.

2.7 Material characterization

A variety of characterizations on active nanocomposites and printed films have been done. These methods were chosen to demonstrate the relationship between materials, printed films properties and sensors results. The results of the characterization techniques on different nanocomposites of the PANI/G have will be presented as well as investigation on the printed films using screen printing and Aerosol-jet printing.

2.7.1 Scanning Electron Microscope (SEM)

Scanning electron microscopes (SEM) are usd to analyze surface topography by scanning the surface of a material using focused stream of electrons which enables access, and exhibit various stages and porosity of the deposited materials layer-by-layer. The microstructures of the active materials films were observed by SEM (JEOL JCM-6000plus, Japan). In this research, SEM is an important characterization technique in order to investigate the specimen topography, microstructure, and also visualize the differences in active materials films depending on the polymer and graphite ratios.

2.7.2 Fourier Transform Infrared Spectroscopy (FTIR)

FTIR stands for “Fourier transform infrared spectroscopy” which is the most common form of infrared spectroscopy. When infrared (IR) radiation passes through a sample, all infrared

spectroscopies work on the principle that some of the radiation are absorbed. As different molecules have different structures and produce different spectra, recording the radiation that passes through the sample can be used to identify the bonds. The spectra are virtually unique, like people's fingerprints or DNA.FTIR is the preferred method of infrared spectroscopy as it has several advantages such as, not destroying the sample, being significantly faster than older techniques, and being much more sensitive and precise.

The benefits of FTIR come from the use of an interferometer, that it is the infrared "source" and allows the Fourier transform and greater speed. The Fourier transform is a mathematical function that separates the waves and returns the frequency of the waves as a function of time. The "output" of the interferometer is not the spectroscopy spectrum that should be used, it is actually a graph known as an "interferogram." The spectrum that we recognize and use is the conversion of the interferogram into the infrared. In Figure 2.9 the FTIR spectrum of PDS initiated polymerization of aniline has been shown.

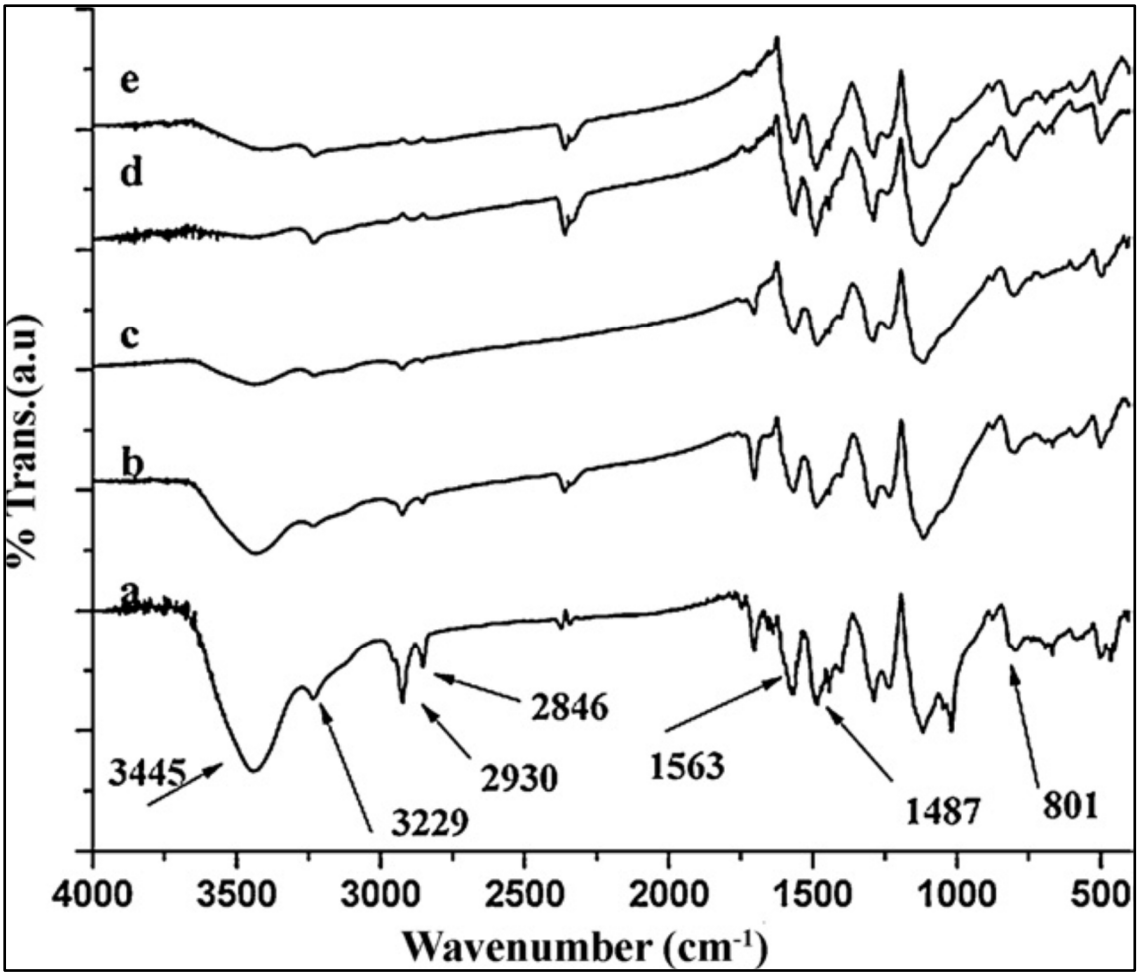

Figure 2.9 FTIR spectrum of PANI–PDS–HCl system (Arasi et al. 2009)

FTIR spectroscopy is used in various sciences such as, polymer science, petrochemical engineering, organic synthesis, food analysis, and pharmaceutical industry. In other words, it has a wide range of applications for monitoring processes, identifying compounds, and determining components in a mixture is needed. Covalent bonds of a molecule selectively absorb radiation of certain wavelengths, which change the vibrational energy of the bond. The type of vibration (stretching or bending) caused by infrared radiation depends on the atoms in the bond. Since different bonds and functional groups absorb at different frequencies, the pass pattern is different for different molecules. The graph of the recorded spectrum is presented with wavenumber (cm^{-1}) recorded on the X-axis and transmittance recorded on the Y-axis. (Wavenumber is 1/wavelength which is corresponds to the energy of the vibration of the molecular bonds) (Anon n.d.-c).

2.7.3 X-Ray diffraction (XRD)

X-Ray diffraction (XRD) analysis is a nondestructive technique which provides detailed information about the chemical composition, crystallographic structure, and physical properties of the materials (Bunaciu, Udriştioiu, and Aboul-Enein 2015). Its foundation is a crystalline sample and the beneficial interference of monochromatic X-rays. When electrically charged particles with enough energy are decelerated, they produce shorter wavelength electromagnetic radiation known as X-rays. For XRD, the produced X-rays are collimated and directed at a sample of nanomaterials. The interaction of the incident rays with the sample results in a diffracted ray, which is then detected, processed, and tallied. A diffraction pattern is visualized by plotting the intensity of diffracted rays scattered at various angles of material. Due to the chemistry and atomic organization of the substance, each phase of the material generates a distinct diffraction pattern. A simple addition of the diffraction patterns from each phase results in the diffraction pattern. The XRD pattern of Polyaniline Emaraldine salt shown in Figure 2.10.

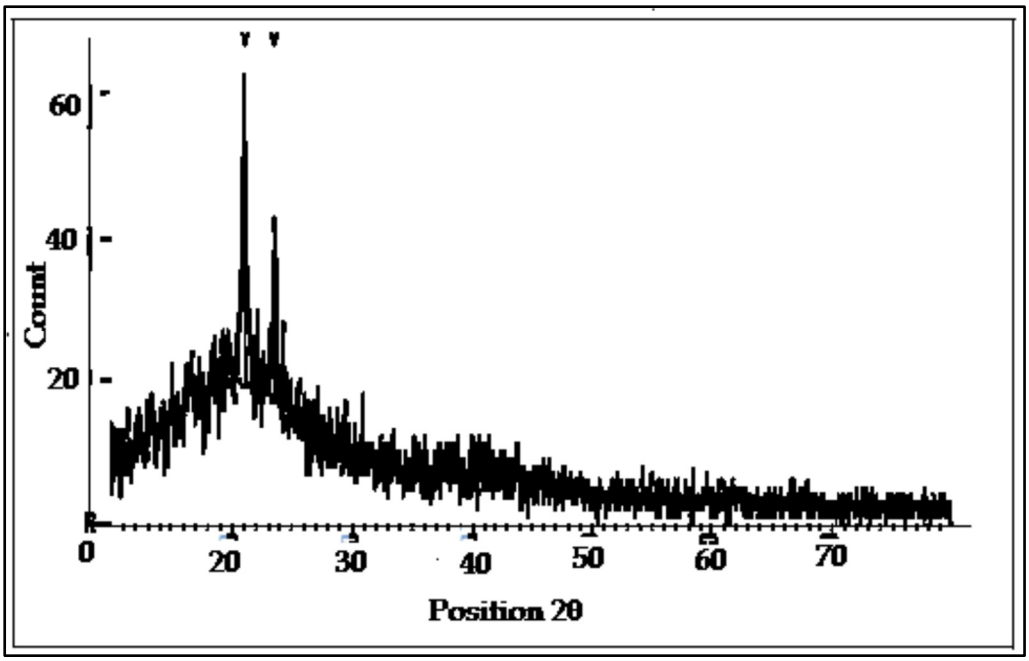

Figure 2.10 XRD pattern of Polyaniline Emaraldine salt (Ameen, Lakshmi, and Husain 2009)

In order to facilitate the phase identification of a material in a wide range of crystalline samples, the qualitative phase analysis of the diffraction pattern of XRD characterization will typically be compared with the established crystallographic databases, such as the International Center for Diffraction Data (ICDD). The peaks of the XRD pattern are crucial for both determining the phases and the characteristics of the nanoparticles. In this instance, the peak's width would reflect the average crystalline size of a nanoparticle, with sharp peaks indicating crystallites of larger sizes and broad peaks indicating crystallites of lesser sizes (Raja et al. 2022).

CHAPTER 3

MATERIALS CHARACTRIZATIONS RESULTS

3.1 SEM

The SEM characterization has been done on the fully scree-printed working electrode pH sensors, the nanocomposite composed of graphite 99.1 wt% and PANI-ES 0.9 wt% exhibited the highest sensitivity and stability for pH levels detection. Unlike the CB paste film which has an inferior porous surface, as seen in Figure 3.1 (a), the addition of PANI-ES significantly enhanced the surface morphology of the G/PANI-ES sensor with a high porosity 3D structure, shown in Figure 3.1 (b). The improvement on the surface area for the G/PANI-ES sensors guaranteed exposure of more reactive sites on the sensor surface that can enhance the sensors' sensitivity.

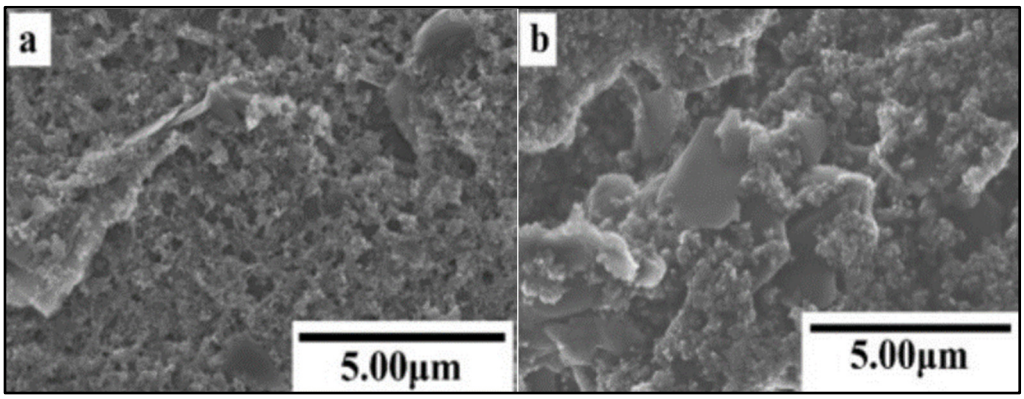

Figure 3.1 SEM images of films printed with (a) pure G paste and (b) nanocomposite composed of G paste 99.1 wt% and PANI-ES 0.9 wt%

The SEM micrographs of PANI/G composites at different ratios are presented in Figure 3.2 showing the attachment of PANI chains on the graphite active sites as well as the graphite being dispersed uniformly in the PANI matrix. It was shown that a large number of PANI covered a small amount of graphite, resulting in flake-like particles. Similar observation was reported by Ju-Lan Zeng and co-workers which emphasized the use of exfoliated graphite nanoplatelets in PANI (Li et al. 2011; Xiang et al. 2010). However, PANI interaction is only

on the exposed layer of the graphite surface which is due to the small interspace of the graphite interlayer.

PANI/G composite solutions printed directly on the Ag/AgCl electrode without the graphite layer is also shown in Figure 3.2 (e-f). The PANI/G composite formed a uniform layer on top of the Ag/AgCl film but there is no visible interaction between PANI chain and Ag/AgCl film as it doesn't have the desired porous morphology and the active sites for potential attachment of PANI chain. In previous reports in which synthesis of PANI/Ag/AgCl nanocomposites was performed, the possible mechanism of the formation of the nanocomposites depended on the synthesis process (Dai 2004). The molar ratio of Ag to Cl^- turned out to be important as unreacted Ag+ serves as the oxidant for the polymerization of aniline. Thus, interactions between polyaniline and Ag/AgCl cannot be obtain by printing the PANI solution directly on top of Ag/AgCl film (Dai 2004).

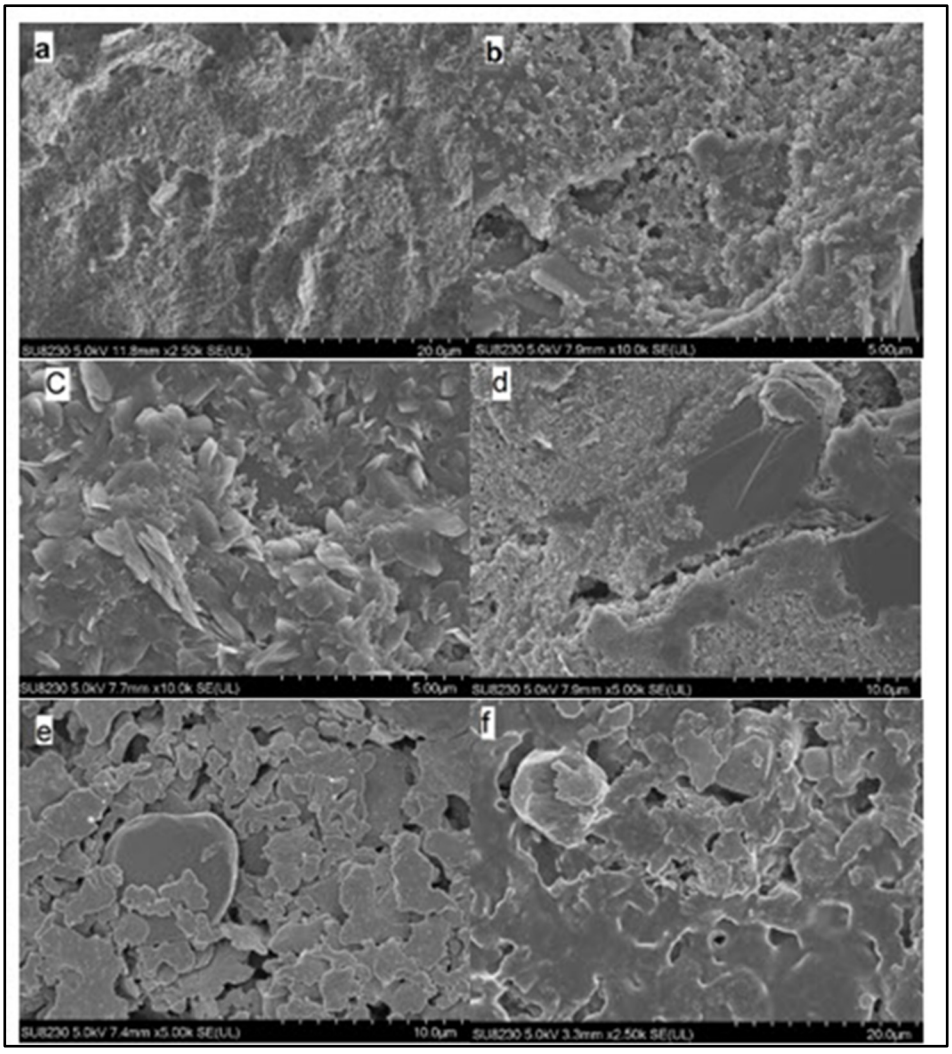

Figure 3.2 SEM images of printed PANI/G composite samples with different graphite loading: (a) graphite, (b) PANI/G 1, (c) PANI/G 2, (d) PANI/G 3, (e) Ag/AgCl, and (f) PANI/G on Ag/AgCl.

3.2 Fourier Transform Infrared (FTIR)

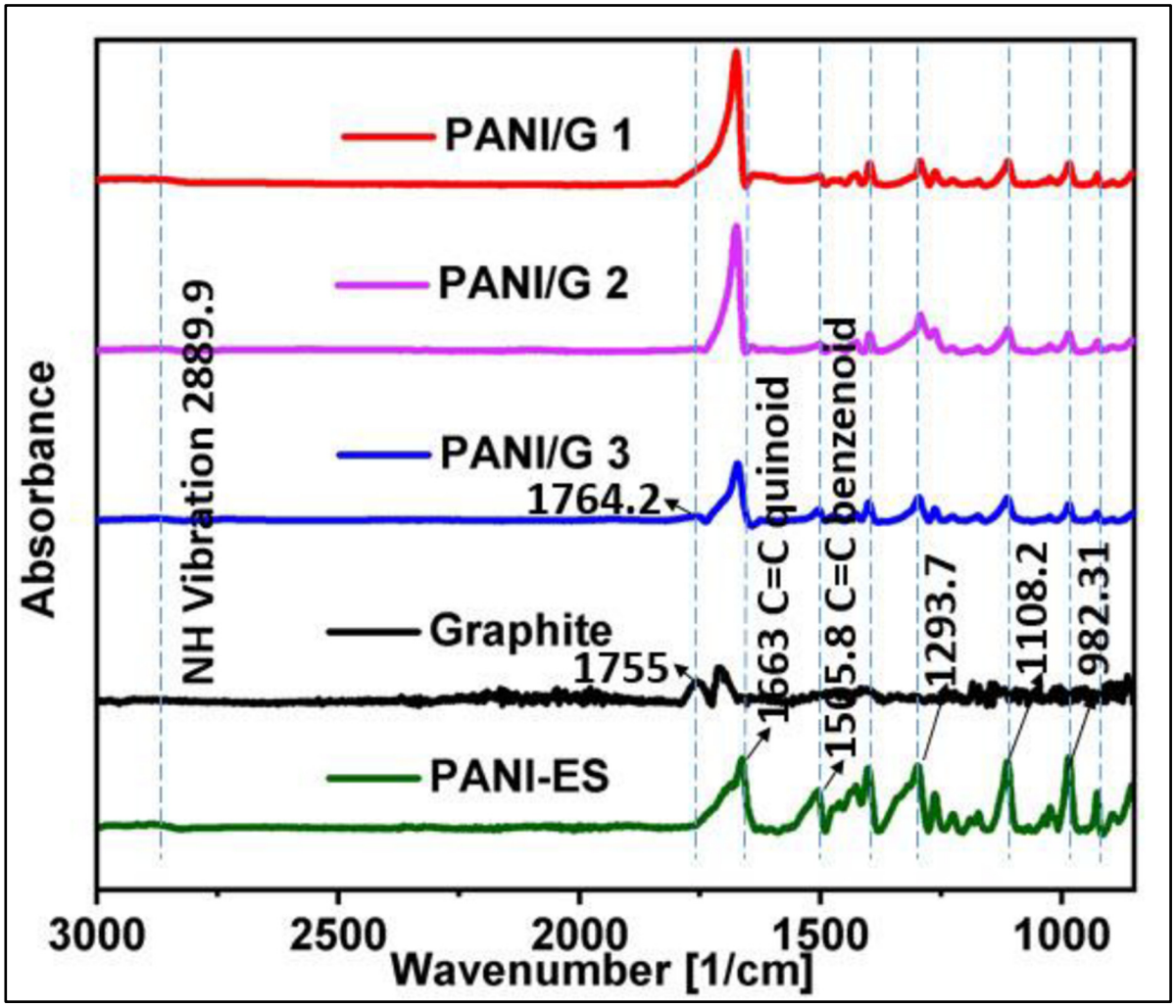

Figure 3.3 FTIR spectra of graphite (G), polyaniline (PANI), PANI/G 1, PANI/G 2, PANI/G 3

The structural changes in the different PANI/G composites have been observed through FTIR spectra, shown in Figure 3.3. The PANI-ES has functional bonding characteristics in the range wavenumber of 400-3000 cm^{-1}. The bonding characteristics formed between 1440-1700 cm^{-1} show the presence of stretched C=C bond of quinoid and benzenoid rings at 1663 and 1505.8 cm^{-1}, respectively. These matches previous reports of characteristic PANI peaks at 1600 cm^{-1} and 1497 $cm^{-}1$ (Diantoro, Masrul, and Taufiq 2018). The peak at 1293.7 cm^{-1} shows the presence of C-N bonds or quinoid rings. This quinoid ring wavenumber indicates the existence

of π electron delocalization which appear through protonation process of polyaniline chain. The C-H in-plane out-of-plane bending vibrations are shown at 1068.7 and 1026 cm^{-1} (Kakde 2017). Also, the PANI-ES peaks at 1263.2, 1108.2, and 747 cm^{-1} correspond to the C–N stretching, C=N stretching, and 1,4-substituted phenyl ring stretching, respectively (Ameen et al. 2009; Holland et al. 1996). There is a shift of peaks and increase of intensities due to interlayer bonding between graphite and PANI. The 1461 cm^{-1} peak corresponds to the C–N stretching vibration which indicates the polaron structure, where PANI in doped state was proven (Holland et al. 1996). The polaron structure leads to energy bands overlapping between the valence and conduction bands, resulting in an increase in conductivity by several orders of magnitude (Ameen, Lakshmi, and Husain 2009; Holland et al. 1996; Yu et al. 2012). Polyaniline chains were attached to the graphite plane resulting for more electron delocalization. Intensities of PANI/G are different at different graphite ratio of graphite and this is due to the N–H bonding in polyaniline and hydroxyl group in graphite. The PANI/G composites intensities increased as the graphite content increased. The intercalation between PANI and graphite would weaken the N–H bonding as the hydroxyl groups prefer to form hydrogen bonds in PANI. Overall, main peaks of PANI at around 2889.9, 1663, 1505.8, and 1293.7 cm^{-1} were exhibited in all PANI/G composite samples. The main peak of graphite at 1755 cm^{-1} appeared in the PANI/G 3 composite with a peak shift to the 1764.2 cm^{-1}. The peaks are shifted from 1108.2 to 1110 cm^{-1} in PANI/G 1, PANI/G 2, and in PANI/G 3 the peak shifted to 1113.2 cm^{-1}. The shift of the peak at the C=N region is due to the lower electron delocalization after de-doping of the PANI chain (Yu et al. 2012). The main reason of the peak shifts is due to the interlayer bonding between graphite and PANI. The intercalation between PANI and graphite lead to weaker N–H bonding as the hydroxyl group prefers to form the hydrogen bond in PANI; which is the reason of less intercalation among PANI and graphite.
The polyaniline chains were anchored by the graphite particles, which resulted in further electron displacement. This explanation was also consistent with the XRD results. Intensities of PANI/G composites were different at the peak around 3000 cm^{-1}. This is attributed to presence of the hydroxyl group in graphite and N–H bonding in polyaniline, respectively. The intensities of PANI/G 3 composite are more than PANI/G 1 and PANI/G 2 in this region which indicate that PANI and graphite were successfully synthesized.

3.3 X-Ray Diffraction Analysis (XRD)

X-ray diffraction (XRD) patterns presented in Figure 3.4 provides an insight into the effect of PANI on the graphite crystal structure.

Some of the features that may be analyzed in XRD patterns of PANI/graphite nanocomposites include:

1. PANI peaks: PANI is an ordered, crystalline material and its XRD pattern should display well-defined peaks that are characteristic of its crystal structure.
2. Graphite peaks: Graphite is a layered material and its XRD pattern should display well-defined peaks at specific angles that are characteristic of its crystal structure.
3. Intercalation peaks: If the graphite has been intercalated into the PANI matrix, the XRD pattern should display additional peaks that are characteristic of the intercalated material.
4. Nanocomposite peaks: The XRD pattern of a PANI/graphite nanocomposite should display a combination of the PANI peaks, the graphite peaks, and any intercalation peaks, providing information about the structure and orientation of the nanocomposite.

The peak shown by PANI was observed at $2\theta = 25.15^{o}$ which corresponded to the (200) plane having orthorhombic structure. In graphite pattern, a sharp peak was observed at $2\theta = 26.58^{o}$. A similar peak has been observed in all forms of carbon composites (Elnaggar et al. 2017). The peak of graphite has been observed in all three PANI/G composites and, as the graphite ratio increased in the composites to 80 wt% in PANI/G 3, the peak of polyaniline also appeared at $2\theta = 25.8^{o}$.

The increase in intensity of the graphite peak at approximately 26–27º in the composites shows that the graphite structure became more crystalline which is referred as the graphite plane. This structure change is due to the charge transfer between the PANI and graphite crystallites, which result in a higher degree of structural ordering in the normal direction to the graphene planes as the atomic positions within the graphene planes become more relaxed (Atiqah et al. 2017). PANI/G 1 exhibited a broad diffraction peak at $2\theta = 26.55^{o}$ suggesting that the composites started to change from partial amorphous to crystalline form by increasing the amount of

graphite into the PANI structure by solution method. The peaks slowly shifted to 2θ = 26.57º in PANI/G 3 as the amount of graphite increased.

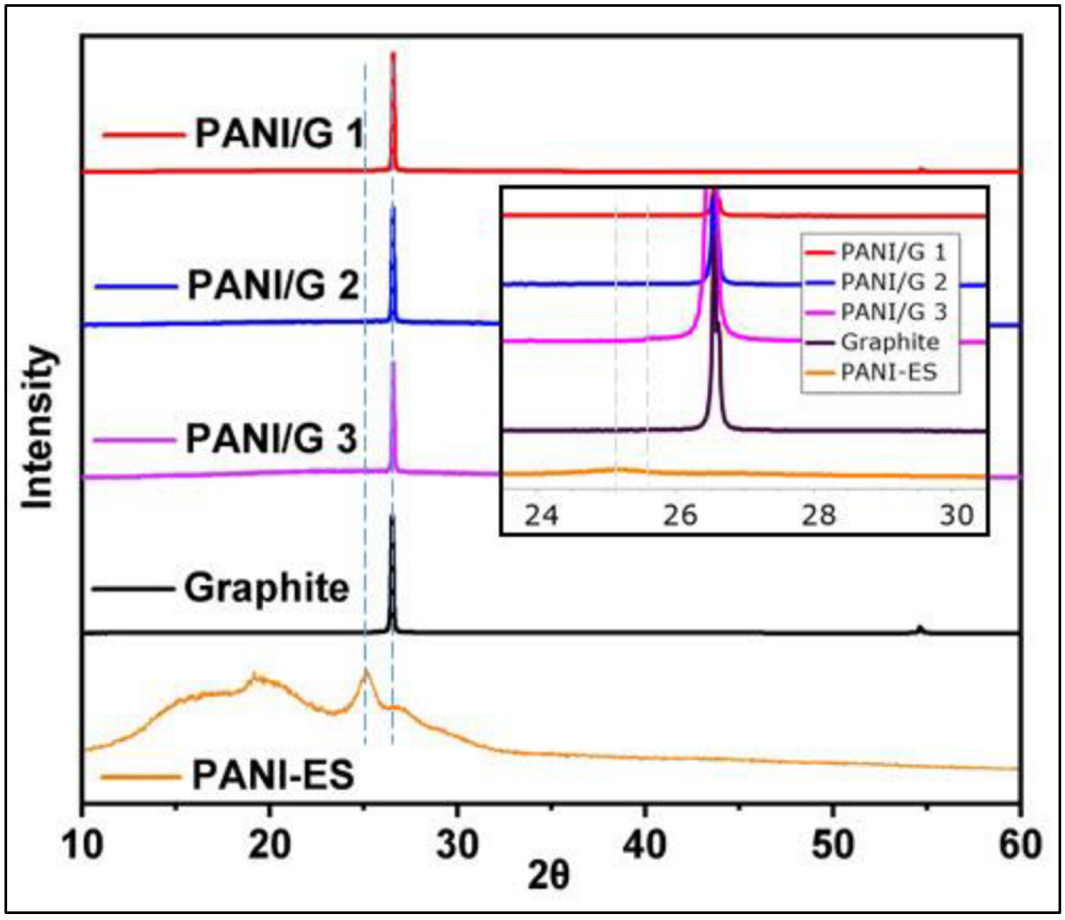

Figure 3.4 XRD pattern of Polyaniline (PANI), Graphite (G), PANI/G 1, PANI/G 2 and PANI/G

CHAPTER 4

POLYANILINE/GRAPHITE pH SENSORS PERFORMANCE

4.1 Fully Screen-printed pH Sensors

The EMF values were measured by immersing the pH sensors in various pH levels solutions ranging from 3 to 11. The pH values of buffered solution were adjusted by adding HCl or NaOH solution to standard buffer solutions (Cole Parmer). In order to control the accuracy of the measurements, the pH values were regularly validated by a commercial pH meter (Accumet AB 15/ 15+ bench-top meter). When immersing the sensors in the buffer solutions, EMF signals changed with varying pH values and reached a steady-state point. EMF measurement results were collected and reported when 85% of steady-state point was reached. Those values are plotted on Figure 4.1 indicating a linear relationship between EMF and pH levels for the printed potentiometric pH sensor.

Based on the Nernst equation, the maximum theoretical sensitivity is -59 mV/pH at room temperature. For the fully screen-printed sensors with the composition of Graphite 99.1 wt% and PANI-ES 0.9 wt% and the thickness of 15 microns as WE, the response is linear with a slope of 50 mV/pH in the wide pH range of 3 to 11, as seen in Figure 4.1 This sensitivity value is close to the Nernstian limit and is comparable to previous reports based on PANI electrodes (Chinnathambi and Euverink 2018; Song and Choi 2014; Zamora et al. 2018). The response time and stability of the pH sensor were evaluated by decreasing the pH level from 7.0 to 3.05 (Figure 4.2). The EMF signal value reached 85% of its steady-state value with a response time of 15 s in acidic and alkaline solutions and remained stable for over 15 min.

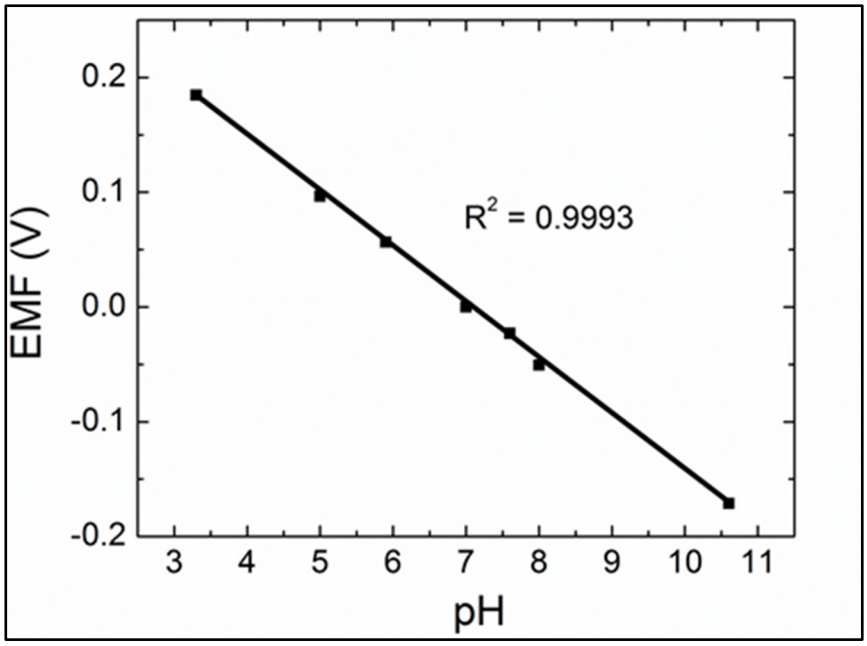

Figure 4.1 Linear EMF responses of the pH sensors measured in various buffer solutions

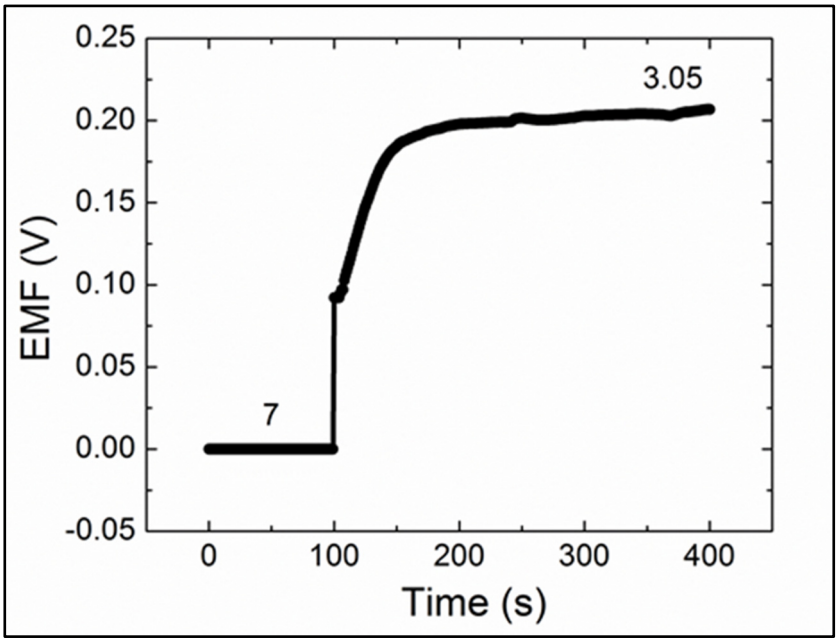

Figure 4.2 EMF response time in titration from pH 7.0 to pH 3.05 for the potentiometric pH sensors

Repeatability is an essential characteristic of an efficient pH sensor which should respond to the changes in pH over different periods of time. The repeatability of pH sensor is indicated in

Figure 4.3 by measuring EMF signals during a reverse titrated-cycle in pH 8.5, 7, 4.1, and 3.05 continuously. To adjust pH values during this process, 1M HCl or NaOH solution was used to decrease or increase pH levels of the buffer. Repeatability test was performed in a wide pH range and over different periods of time without washing and drying the sensor between immersions. A slight decrease in sensitivity from 50 mV/pH to 48.5 mV/pH was observed after the fifth cycle due to a potential degradation and wetting of the active layers.

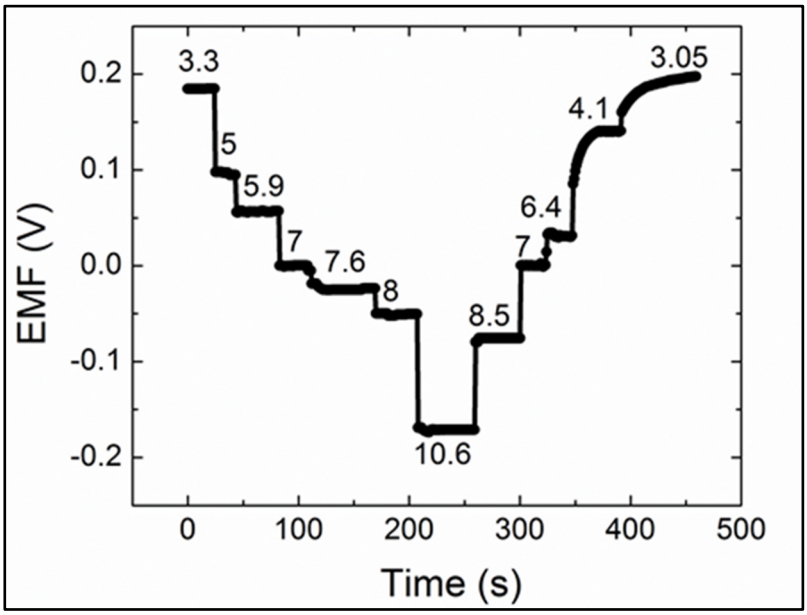

Figure 4.3 Repeatability test for pH CB/PANI-ES sensor in the pH ranged from 3 to 11

4.2 pH Sensors Modified with Aerosol-jet Printing

Both pH sensitivity and stability were different in sensors with a screen-printed graphite layer modified with PANI/G 1, PANI/G 2 and PANI/G 3 (Table 2.2.3) in different number of layers from 3 to 10 layers of printing with same parameters and the sensors modified with 5 layers of the active nanocomposites showed better results and the aerosol-jet printed active materials (PANI/G 3 nanocomposites) on top of screen-printed graphite showed in Figure 4.5,and all the results that will be presented are related to these sensors.

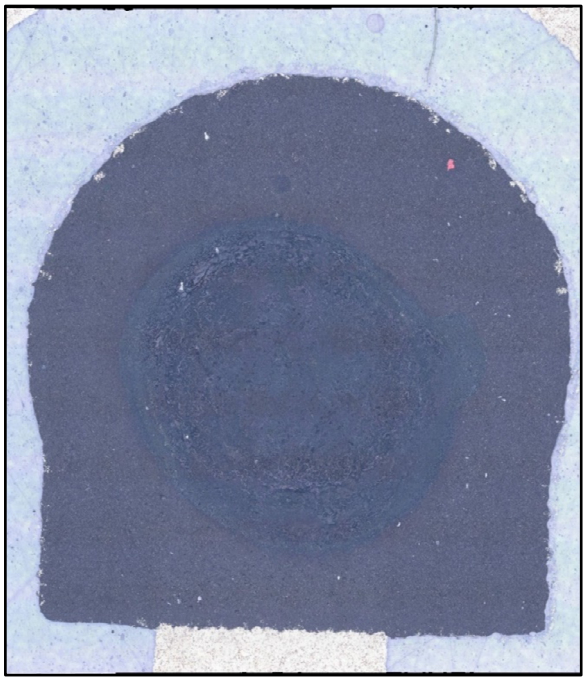

Figure 4.4 Aerosol-jet printed sensing material
on working electrode

The sensors functionality improved as the ratio of graphite increased in the composites. The EMF measurement between the working electrode and the Ag/AgCl reference electrode provides electrochemical characteristics of the potentiometric pH sensor. The EMF values were measured by immersing the pH sensors in various pH levels solutions ranging from 3 to 11. When immersing the sensors in the buffer solutions, EMF signals changed with varying pH values and reached a steady-state point. EMF measurement results were collected and reported when 85% of steady-state point was reached and the stability duration reported for time the voltage remained stable (Figure 4.4).

The sensors modified with PANI/G 1 composite exhibited 25 mV/pH sensitivity and a stability of 30 s when tested in different pH levels with various cycles (Figure 4.5 (a)). The sensors modified with PANI/G 2 composite exhibited a better sensitivity and stability of 40 mV/pH and 50 s, respectively (Figure 4.5 (b)). The sensors modified with PANI/G 3 composite reached a near-Nernstian sensitivity of 53 mV/pH and about 2 minutes stability (Figure 4.5 (c)-Figure 4.6 (a)).

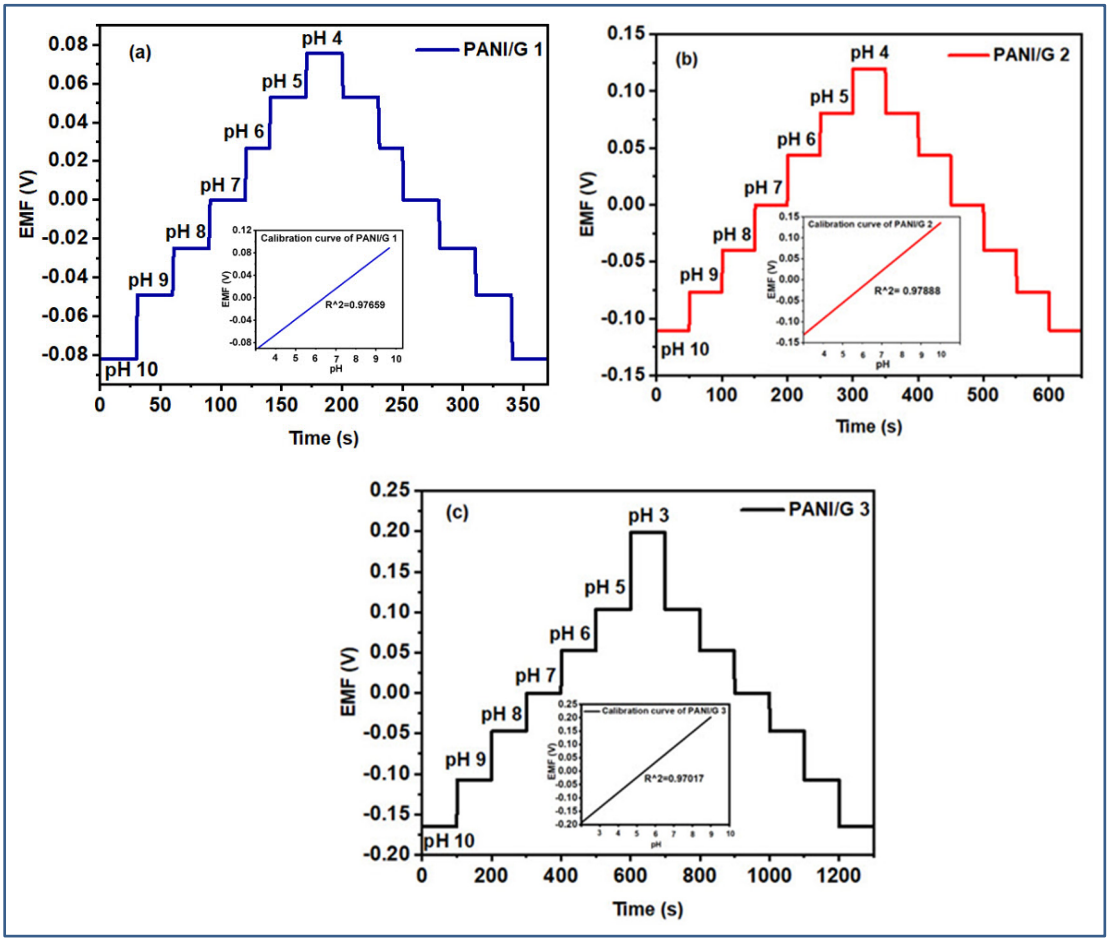

Figure 4.5 Sensitivity and Repeatability test for pH from the sensors fabricated from (a) PANI/G 1, (b) PANI/G 2 and (c) PANI/G 3 composites in the pH range from 3 to 10

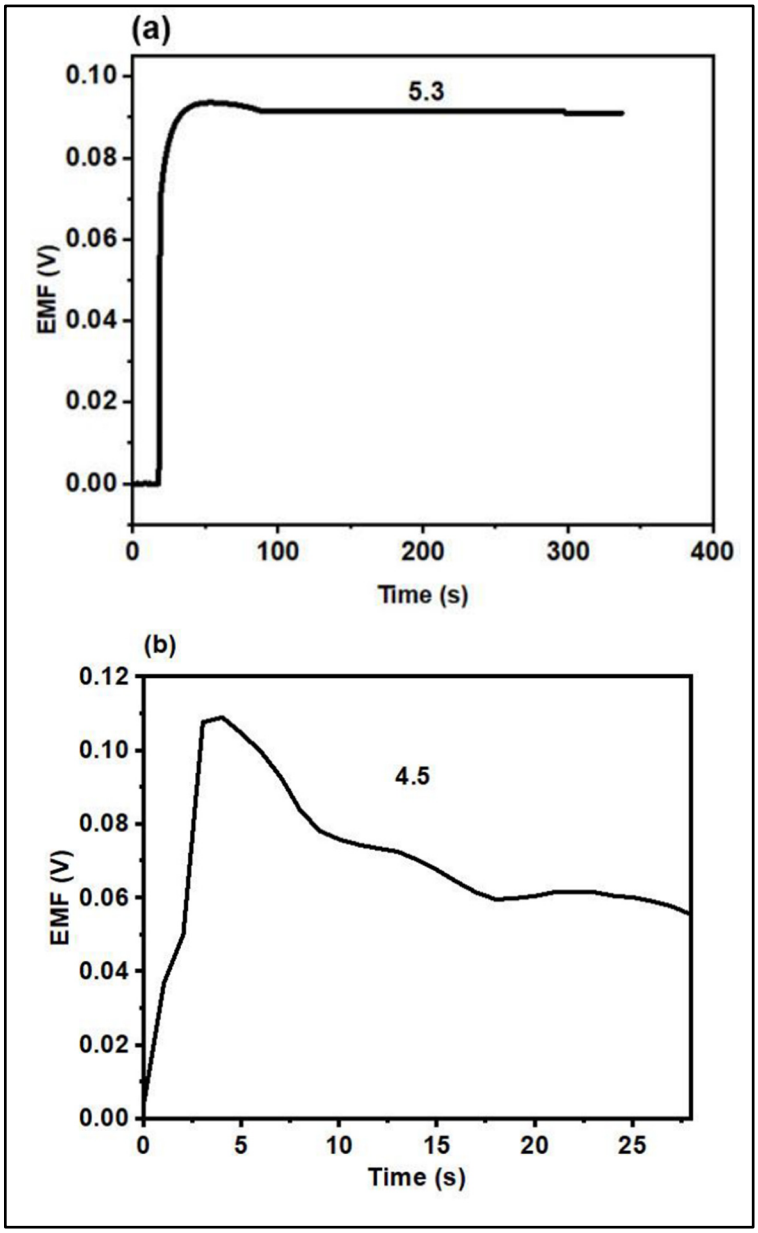

Figure 4.6 Stability and response time test for (a) the sensor modified with PANI/G 3 composite printed on the graphite layer and (b) the sensor modified with PANI/G 3 composite printed directly on Ag/AgCl electrode without graphite layer

The PANI/G 3 composite which exhibited the most promising result was then deposited on Ag/AgCl electrode without the graphite layer to investigate its role in sensitivity and stability of the sensor. The sensors modified with PANI/G 3 composite on Ag/AgCl electrode without

the graphite layer showed the sensitivity of about 33 mV/pH. The response time of the sensor fabricated with all three compositions was fast and on average at 15 s, but the stability (Figure 4.6 (b)-Figure 4.7) was much lower than the sensors with the graphite layer and the voltage dropped after an average time of 10 s, which could be due to the insufficient active sites on the surface of Ag/AgCl film for successful attachment of the PANI chain in compare to graphite film as showed in SEM characterization.

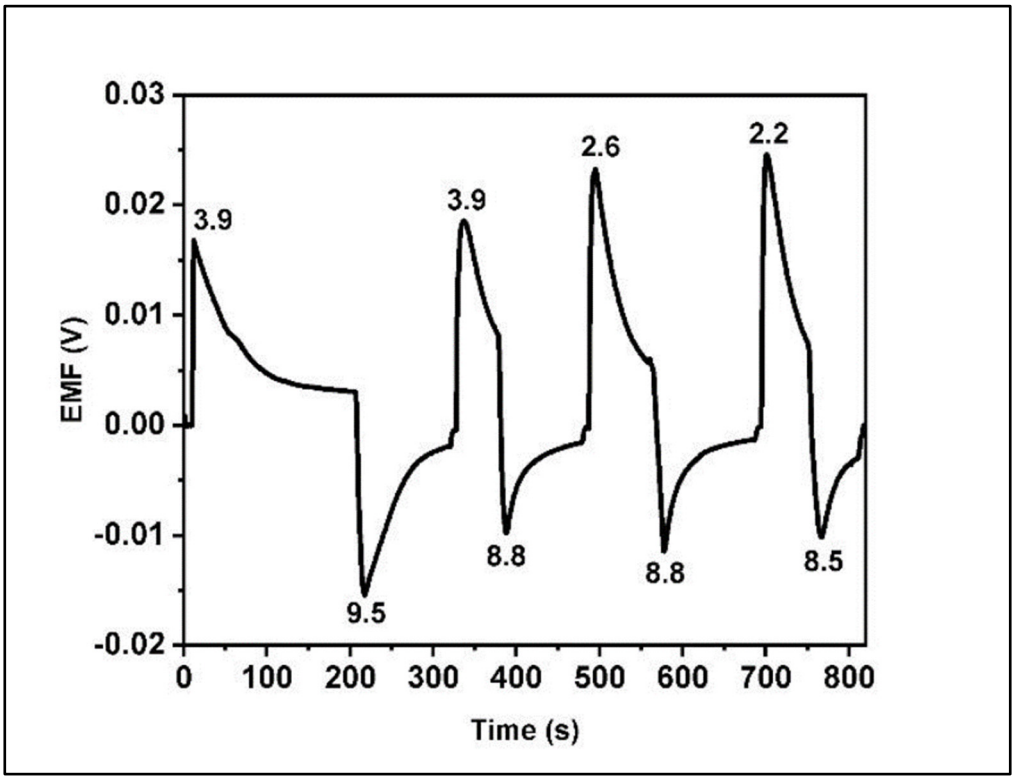

Figure 4.7 Repeatability of the sensor modified with PANI/G 3 composite

One of the most important factors for potentiometric pH sensors is the selectively, which refers to its ability to distinguish hydrogen ions (H^+) from other interfering ions in the solution being measured. A high selectivity for H^+ is important for accurate pH measurement as it reduces the influence of interfering ions on the measurement. The selectivity of a potentiometric pH sensor is often characterized by its "K value", which represents the ratio of the response of the electrode to changes in hydrogen ion concentration compared to changes in concentration of other ions. A low K value indicates high selectivity for H^+.

In this study, we selected some of the ions in that are present in blood as they are important in preventing blood cells and can interfere with H_3O^+ ion while measuring the pH. Separate-solution method (SSM) has been used to evaluate selectivity coefficients of pH sensors against different interfering ions of K^+, Na^+, Ca^{2+}, Zn^+ and $[PO_4]^{3-}$. The EMF responses were measured in different solutions containing every ion at a same concentration of 3 M. The selectivity coefficient (K_{AB}^{POT}) in SSM can be calculated as follows (Park et al. 2019):

$$\log k_{AB}^{POT} = \frac{(E_B - E_A)Z_A F}{2.03RT} + \left(1 - \frac{Z_A}{Z_B}\right)\log a_A \quad (4.1)$$

Where K_{AB}^{POT} is the potentiometric selectivity coefficient for ion B with respect to the primary ion A, E is the experimentally determined galvanic potential difference of ISE cell (in V), R is the gas constant equal to 8.314510 J $K^{-1}mol^{-1}$, T is the absolute temperature in K, F is the Faraday constant, $9.6485309x10^4$ C mol^{-1}, a_A is the activity of ion A and Z is the charge number of every ion. The measured K values of pH sensor fabricated with PANI/G 3 composite are shown in Table 4.1. All of the K values for pH sensor are below 10^{-9} which indicates that the sensor has a high selectivity for hydrogen ions (H^+) over other ions in the solution being measured.

Table 4.1 Selective coefficients of pH sensors using SSM for primary ion (H^+) against interfering ions.

Ions	**log K^{POT}_{AB}**	**K^{POT}_{AB}**
K^+	-8.609	2.46×10^{-9}
Na^+	-8.501	3.15×10^{-9}
Ca^{2+}	-9.026	9.41×10^{-10}
Zn^+	-9.044	9.03×10^{-10}
$[PO_4]^{3-}$	-9.809	1.55×10^{-10}

CONCLUSION

We fabricated a flexible and fully printed pH sensor using a screen printing process with G/PANI-ES as a working electrode and Ag/AgCl as a reference electrode. The screen printing technique provided a high-throughput and straightforward fabrication process for the pH sensors while the direct addition of PANI-ES to the G paste provided an efficient way to deposit the active material without electrodeposition. Properties of the pH sensor were characterized in terms of sensitivity, response time, stability, and repeatability. The pH sensor exhibited a sensitivity of 50 mV/pH that was near the maximum Nernstian limit, a fast response time of 15 s, good linearity in pH scale between 3 to 11, good reproducibility, and suitable repeatability were observed. This fully printed potentiometric pH sensor has the potential to be implemented in many applications, including health monitoring, water treatment, and food packaging.

In order to investigate the effect of graphite in active composites on the functionality of the sensors, the working electrode has been modified with PANI/G composites using Aerosol-jet printing which is more flexible in terms of the range of the viscosity of the materials could be printed. PANI/G composites have been characterized to investigate the effect of graphite loading in active composites on sensitivity and stability of the sensors. As potentiometry is a robust technique sensors fabricated with all compositions had a fast response time of 15 s and as the graphite loading increased the functionality of the sensor in terms sensitivity and stability improved and sensors modified with PANI/G 3 (PANI %20, Graphite %80) exhibited a sensitivity of 53 mV/pH and performed a good repeatability and selectivity.

.

RECOMMENDATION FOR FUTURE WORK

The stability of the reference electrode is a significant challenge in development of printed pH sensors. The reference electrode should be repeatable, keeps a constant potential throughout device operation, and also be insensitive to changes in the testing environment. The reference electrode also plays a crucial role in defining the repeatability and accuracy of the sensor measurements. To optimize the reference electrode and increase the stability of the sensor the $Ag|AgCl|Cl^-$ reference electrode could be fabricated by printing a KCl (3 M) layer on top of the Ag/AgCl reference (Shinwari et al. 2010; Sibug-Torres, Go, and Enriquez 2020).

A fully screen-printed three-electrode pH sensor can also be designed and fabricated in order to compare with the two-electrode system and increase the stability with adding the counter electrode. The flexibility of the sensors can be characterized as well as investigation of stretchable substrates which will be beneficial for using the sensors in smart bandage application.

LIST OF BIBLIOGRAPHICAL REFERENCES

Agarwala, Shweta, Guo Liang Goh, Yee Ling Yap, Guo Dong Goh, Hao Yu, Wai Yee Yeong, and Tuan Tran. 2017. "Development of Bendable Strain Sensor with Embedded Microchannels Using 3D Printing." *Sensors and Actuators A: Physical* 263:593–99.

Alam, Arif Ul, Yiheng Qin, Shruti Nambiar, John T. W. Yeow, Matiar M. R. Howlader, Nan-Xing Hu, and M. Jamal Deen. 2018. "Polymers and Organic Materials-Based PH Sensors for Healthcare Applications." *Progress in Materials Science* 96:174–216. doi: 10.1016/j.pmatsci.2018.03.008.

Ameen, Sadia, GBVS Lakshmi, and M. Husain. 2009. "Synthesis and Characterization of Polyaniline Prepared with the Dopant Mixture of (ZrO2/PbI2)." *Journal of Physics D: Applied Physics* 42(10):105104.

Anon. n.d.-a. "Intracellular PH | Circulation." Retrieved December 9, 2022 (https://www.ahajournals.org/doi/10.1161/CIRCULATIONAHA.111.061226).

Anon. n.d.-b. "Screen Printed Cupric-Hexacyanoferrate Modified Carbon Enzyme Electrode for Single-Use Glucose Measurements | Request PDF." Retrieved December 9, 2022 (https://www.researchgate.net/publication/239246036_Screen_Printed_Cupric-Hexacyanoferrate_Modified_Carbon_Enzyme_Electrode_for_Single-Use_Glucose_Measurements?_iepl%5BgeneralViewId%5D=FisivYCBUoMhQ4fp1066mnC6vY8bcaJuwiyV&_iepl%5Bcontexts%5D%5B0%5D=searchReact&_iepl%5BviewId%5D=Pq5o6hSWEoGsQjSwLKL40U4zw0D03NxcTM1E&_iepl%5BsearchType%5D=publication&_iepl%5Bdata%5D%5BcountLessEqual20%5D=1&_iepl%5Bdata%5D%5BinteractedWithPosition2%5D=1&_iepl%5Bdata%5D%5BwithoutEnrichment%5D=1&_iepl%5Bposition%5D=2&_iepl%5BrgKey%5D=PB%3A239246036&_iepl%5BtargetEntityId%5D=PB%3A239246036&_iepl%5BinteractionType%5D=publicationTitle).

Anon. n.d.-c. "What Is FTIR Spectroscopy?" Retrieved November 28, 2022 (https://www.sigmaaldrich.com/CA/en/technical-documents/technical-article/analytical-chemistry/photometry-and-reflectometry/ftir-spectroscopy?msclkid=7c185494b2ca1936dbe3364949647804&utm_source=bing&utm_medium=cpc&utm_campaign=all%20substances_dsa_bing_(ebizpfs)&utm_term=product%20aldrich%20&utm_content=all%20substances).

Arasi, A. Yelil, J. Juliet Latha Jeyakumari, B. Sundaresan, V. Dhanalakshmi, and R. Anbarasan. 2009. "The Structural Properties of Poly (Aniline)—Analysis via FTIR Spectroscopy." *Spectrochimica Acta Part A: Molecular and Biomolecular Spectroscopy* 74(5):1229–34.

Arrabito, Giuseppe, Yana Aleeva, Riccardo Pezzilli, Vittorio Ferrara, Pier Gianni Medaglia, Bruno Pignataro, and Giuseppe Prestopino. 2020. “Printing ZnO Inks: From Principles to Devices.” *Crystals* 10(6):449.

Atiqah, T. N., Soo Jin Tan, Kai Loong Foo, A. G. Supri, and M. F. Abdullah. 2017. “Structural and Electrical Properties of Graphite in Polyaniline/Graphite (PANI/G) Composites.” *Materials Science Forum* 889:9–13. doi: 10.4028/www.scientific.net/MSF.889.9.

Bandodkar, Amay J., Vinci W. S. Hung, Wenzhao Jia, Gabriela Valdés-Ramírez, Joshua R. Windmiller, Alexandra G. Martinez, Julian Ramírez, Garrett Chan, Kagan Kerman, and Joseph Wang. 2013. “Tattoo-Based Potentiometric Ion-Selective Sensors for Epidermal PH Monitoring.” *The Analyst* 138(1):123–28. doi: 10.1039/c2an36422k.

Bariya, Mallika, Ziba Shahpar, Hyejin Park, Junfeng Sun, Younsu Jung, Wei Gao, Hnin Yin Yin Nyein, Tiffany Sun Liaw, Li-Chia Tai, and Quynh P. Ngo. 2018. “Roll-to-Roll Gravure Printed Electrochemical Sensors for Wearable and Medical Devices.” *ACS Nano* 12(7):6978–87.

Bellew, Allen T., Alan P. Bell, Eoin K. McCarthy, Jessamyn A. Fairfield, and John J. Boland. 2014. “Programmability of Nanowire Networks.” *Nanoscale* 6(16):9632–39.

Bobacka, Johan, Zhiqiang Gao, Ari Ivaska, and Andrzej Lewenstam. 1994. “Mechanism of Ionic and Redox Sensitivity of P-Type Conducting Polymers: Part 2. Experimental Study of Polypyrrole.” *Journal of Electroanalytical Chemistry* 368(1):33–41. doi: 10.1016/0022-0728(93)03081-Y.

Buck, Richard P., and Erno Lindner. 1994. “Recommendations for Nomenclature of Ionselective Electrodes (IUPAC Recommendations 1994).” *Pure and Applied Chemistry* 66(12):2527–36.

Bunaciu, Andrei A., Elena gabriela Udriştioiu, and Hassan Y. Aboul-Enein. 2015. “X-Ray Diffraction: Instrumentation and Applications.” *Critical Reviews in Analytical Chemistry* 45(4):289–99. doi: 10.1080/10408347.2014.949616.

Cao, Xuan, Christian Lau, Yihang Liu, Fanqi Wu, Hui Gui, Qingzhou Liu, Yuqiang Ma, Haochuan Wan, Moh R. Amer, and Chongwu Zhou. 2016. “Fully Screen-Printed, Large-Area, and Flexible Active-Matrix Electrochromic Displays Using Carbon Nanotube Thin-Film Transistors.” *ACS Nano* 10(11):9816–22.

Carrilho, Emanuel, Scott T. Phillips, Sarah J. Vella, Andres W. Martinez, and George M. Whitesides. 2009. “Paper Microzone Plates.” *Analytical Chemistry* 81(15):5990–98.

Chen, Aicheng, and Sanghamitra Chatterjee. 2013. “Nanomaterials Based Electrochemical Sensors for Biomedical Applications.” *Chemical Society Reviews* 42(12):5425–38.

Chinnathambi, Selvaraj, and Gert Jan Willem Euverink. 2018. “Polyaniline Functionalized Electrochemically Reduced Graphene Oxide Chemiresistive Sensor to Monitor the PH in Real Time during Microbial Fermentations.” *Sensors and Actuators B: Chemical* 264:38–44. doi: 10.1016/j.snb.2018.02.087.

Chu, Jian, Yue Zhao, Shu-Hong Li, Han-Qing Yu, Gang Liu, and Yang-Chao Tian. 2015. “An Integrated Solid-State PH Microelectrode Prepared Using Microfabrication.” *Electrochimica Acta* 152:6–12.

Da Costa, Tallis H., Edward Song, Ryan P. Tortorich, and Jin-Woo Choi. 2015. “A Paper-Based Electrochemical Sensor Using Inkjet-Printed Carbon Nanotube Electrodes.” *ECS Journal of Solid State Science and Technology* 4(10):S3044.

Dai, Liming. 2004. *Intelligent Macromolecules for Smart Devices: From Materials Synthesis to Device Applications*. Springer Science & Business Media.

Douglas, P., and K. Eaton. 2002. “Response Characteristics of Thin Film Oxygen Sensors, Pt and Pd Octaethylporphyrins in Polymer Films.” *Sensors and Actuators B: Chemical* 82(2–3):200–208.

Elnaggar, Elsayed M., Khalid I. Kabel, Ahmed A. Farag, and Abdalrhman G. Al-Gamal. 2017. “Comparative Study on Doping of Polyaniline with Graphene and Multi-Walled Carbon Nanotubes.” *Journal of Nanostructure in Chemistry* 7(1):75–83.

Gao, Wei, Sam Emaminejad, Hnin Yin Yin Nyein, Samyuktha Challa, Kevin Chen, Austin Peck, Hossain M. Fahad, Hiroki Ota, Hiroshi Shiraki, and Daisuke Kiriya. 2016. “Fully Integrated Wearable Sensor Arrays for Multiplexed in Situ Perspiration Analysis.” *Nature* 529(7587):509–14.

Geniès, E. M., A. Boyle, M. Lapkowski, and C. Tsintavis. 1990. “Polyaniline: A Historical Survey.” *Synthetic Metals* 36(2):139–82. doi: 10.1016/0379-6779(90)90050-U.

Gill, Edric, Khalil Arshak, Arousian Arshak, and Olga Korostynska. 2008. “Mixed Metal Oxide Films as PH Sensing Materials.” *Microsystem Technologies* 14(4):499–507.

Hart, A. L., A. P. F. Turner, and D. Hopcroft. 1996. “On the Use of Screen-and Ink-Jet Printing to Produce Amperometric Enzyme Electrodes for Lactate.” *Biosensors and Bioelectronics* 11(3):263–70.

Hickman, James J., David Ofer, Paul E. Laibinis, George M. Whitesides, and Mark S. Wrighton. 1991. “Molecular Self-Assembly of Two-Terminal, Voltammetric Microsensors with Internal References.” *Science* 252(5006):688–91.

Holland, E. R., S. J. Pomfret, P. N. Adams, and A. P. Monkman. 1996. “Conductivity Studies of Polyaniline Doped with CSA.” *Journal of Physics: Condensed Matter* 8(17):2991.

Jabbour, Ghassan E., Rachel Radspinner, and Nasser Peyghambarian. 2001. “Screen Printing for the Fabrication of Organic Light-Emitting Devices.” *IEEE Journal of Selected Topics in Quantum Electronics* 7(5):769–73.

Jović, Milica, Jonnathan C. Hidalgo-Acosta, Andreas Lesch, Victor Costa Bassetto, Evgeny Smirnov, Fernando Cortés-Salazar, and Hubert H. Girault. 2018. “Large-Scale Layer-by-Layer Inkjet Printing of Flexible Iridium-Oxide Based PH Sensors.” *Journal of Electroanalytical Chemistry* 819:384–90.

Kadara, Rashid O., Norman Jenkinson, and Craig E. Banks. 2009. “Characterisation of Commercially Available Electrochemical Sensing Platforms.” *Sensors and Actuators B: Chemical* 138(2):556–62.
Kadara, Rashid O., Norman Jenkinson, Bo Li, Kenneth H. Church, and Craig E. Banks. 2008. “Manufacturing Electrochemical Platforms: Direct-Write Dispensing versus Screen Printing.” *Electrochemistry Communications* 10(10):1517–19.

Kahlert, Heike. 2008. “Functionalized Carbon Electrodes for PH Determination.” *Journal of Solid State Electrochemistry* 12(10):1255–66.

Karyakin, A. A., M. Vuki, L. V. Lukachova, E. E. Karyakina, A. V. Orlov, G. P. Karpachova, and J. Wang. 1999. “Processible Polyaniline as an Advanced Potentiometric PH Transducer. Application to Biosensors.” *Analytical Chemistry* 71(13):2534–40. doi: 10.1021/ac981337a.

Karyakin, Arkady A., Oksana A. Bobrova, Lylia V. Lukachova, and Elena E. Karyakina. 1996. “Potentiometric Biosensors Based on Polyaniline Semiconductor Films.” *Sensors and Actuators B: Chemical* 33(1):34–38. doi: 10.1016/0925-4005(96)01929-6.

Khan, Saleem. 2016. “Towards Merging of Microfabrication and Printing of Si M-Wires for Flexible Electronics.” phd, University of Trento.

Khan, Saleem, Leandro Lorenzelli, and Ravinder S. Dahiya. 2014. “Technologies for Printing Sensors and Electronics over Large Flexible Substrates: A Review.” *IEEE Sensors Journal* 15(6):3164–85.

Kishore, Chandra, Kanagesan Samikannu, Raji Atchudan, suguna perumal, Thomas Edison, Muthulakshmi Alagan, Ashok Sundramoorthy, and Yong Lee. 2022. “Smartphone-Operated Wireless Chemical Sensors: A Review.” *Chemosensors* 10:55. doi: 10.3390/chemosensors10020055.

Korostynska, Olga, Khalil Arshak, Edric Gill, and Arousian Arshak. 2007. “State Key Laboratory of Nonlinear Mechanics (LNM), Institute of Mechanics, Chinese Academy of Sciences, Beijing 100080, China.” *Sensors* 7(12):3027.

Kumar, A. Akshaya, SK Naveen Kumar, and Almaw Ayele Aniley. 2021. “Fabrication of Interdigitated Electrodes (IDEs) by Screen Printing Technology and Their Structural Studies.” Pp. 77–87 in *Nanostructured Smart Materials*. Apple Academic Press.

Lafitte, Valerie GH, Wanxian Wang, Alexandra S. Yashina, and Nathan S. Lawrence. 2008. “Anthraquinone–Ferrocene Film Electrodes: Utility in PH and Oxygen Sensing.” *Electrochemistry Communications* 10(12):1831–34.

Lamas-Ardisana, Pedro J., Pablo Casuso, Ivan Fernandez-Gauna, Graciela Martínez-Paredes, Elena Jubete, Larraitz Añorga, Germán Cabañero, and Hans J. Grande. 2017. “Disposable Electrochemical Paper-Based Devices Fully Fabricated by Screen-Printing Technique.” *Electrochemistry Communications* 75:25–28.

Lasia, Andrzej. 2002. “Electrochemical Impedance Spectroscopy and Its Applications.” Pp. 143–248 in *Modern aspects of electrochemistry*. Springer.

Lawrence, Nathan S., Markus Pagels, Simon FJ Hackett, Sean McCormack, Andrew Meredith, Timothy GJ Jones, Gregory G. Wildgoose, Richard G. Compton, and Li Jiang. 2007. “Triple Component Carbon Epoxy PH Probe.” *Electroanalysis: An International Journal Devoted to Fundamental and Practical Aspects of Electroanalysis* 19(4):424–28.

Leventis, Henry C., Ian Streeter, Gregory G. Wildgoose, Nathan S. Lawrence, Li Jiang, Timothy GJ Jones, and Richard G. Compton. 2004. “Derivatised Carbon Powder Electrodes: Reagentless PH Sensors.” *Talanta* 63(4):1039–51.

Li, Ji Hui, Mei Li, Qian Liu, and Hui Fang Da. 2011. “Preparation and Characterization of Polyaniline/Exfoliated Graphite Composite via a Combination Method of in Situ Polymerization and Thermal Expansion.” *Journal of Materials Science: Materials in Electronics* 22(8):1016–20.

Li, Xiao, Man Zhang, Yujie Hu, Jian Xu, Dongke Sun, Tao Hu, and Zhonghua Ni. 2020. “Screen-Printed Electrochemical Biosensor Based on a Ternary Co@ MoS2/RGO Functionalized Electrode for High-Performance Non-Enzymatic Glucose Sensing.” *Biomedical Microdevices* 22(1):1–8.

Lindfors, Tom, and Ari Ivaska. 2002. “PH Sensitivity of Polyaniline and Its Substituted Derivatives.” *Journal of Electroanalytical Chemistry* 531(1):43–52. doi: 10.1016/S0022-0728(02)01005-7.

Lowe, Benjamin M., Kai Sun, Ioannis Zeimpekis, Chris-Kriton Skylaris, and Nicolas G. Green. 2017. “Field-Effect Sensors–from PH Sensing to Biosensing: Sensitivity Enhancement Using Streptavidin–Biotin as a Model System.” *Analyst* 142(22):4173–4200.

Lvovich, Vadim F. 2012. *Impedance Spectroscopy: Applications to Electrochemical and Dielectric Phenomena*. John Wiley & Sons.

Määttänen, Anni, Ulriika Vanamo, Petri Ihalainen, Petri Pulkkinen, Heikki Tenhu, Johan Bobacka, and Jouko Peltonen. 2013. "A Low-Cost Paper-Based Inkjet-Printed Platform for Electrochemical Analyses." *Sensors and Actuators B: Chemical* 177:153–62.

Mahinnezhad, Shirin, Homa Emami, Mohsen Ketabi, Ahmad Al Shboul, Najet Belkhamssa, Andy Shih, and Ricardo Izquierdo. 2021. "Fully Printed PH Sensor Based in Carbon Black/Polyaniline Nanocomposite." Pp. 1–4 in *2021 IEEE Sensors*. IEEE.

Manjakkal, Libu, Katarina Cvejin, Branimir Bajac, Jan Kulawik, Krzysztof Zaraska, and Dorota Szwagierczak. 2015. "Microstructural, Impedance Spectroscopic and Potentiometric Analysis of Ta2O5 Electrochemical Thick Film PH Sensors." *Electroanalysis* 27(3):770–81.

Manjakkal, Libu, Katarina Cvejin, Jan Kulawik, Krzysztof Zaraska, Robert P. Socha, and Dorota Szwagierczak. 2016. "X-Ray Photoelectron Spectroscopic and Electrochemical Impedance Spectroscopic Analysis of RuO2-Ta2O5 Thick Film PH Sensors." *Analytica Chimica Acta* 931:47–56.

Manjakkal, Libu, Katarina Cvejin, Jan Kulawik, Krzysztof Zaraska, and Dorota Szwagierczak. 2014. "A Comparative Study of Potentiometric and Conductimetric Thick Film PH Sensors Made of RuO2 Pastes." *Sensor Letters* 12(11):1645–50.

Manjakkal, Libu, Katarina Cvejin, Jan Kulawik, Krzysztof Zaraska, Dorota Szwagierczak, and Goran Stojanovic. 2015. "Sensing Mechanism of RuO2–SnO2 Thick Film PH Sensors Studied by Potentiometric Method and Electrochemical Impedance Spectroscopy." *Journal of Electroanalytical Chemistry* 759:82–90.

Manjakkal, Libu, Saoirse Dervin, and Ravinder Dahiya. 2020. "Flexible Potentiometric PH Sensors for Wearable Systems." *RSC Advances* 10(15):8594–8617.

Manjakkal, Libu, Elvira Djurdjic, Katarina Cvejin, Jan Kulawik, Krzysztof Zaraska, and Dorota Szwagierczak. 2015. "Electrochemical Impedance Spectroscopic Analysis of RuO2 Based Thick Film PH Sensors." *Electrochimica Acta* 168:246–55.

Manjakkal, Libu, Beata Synkiewicz, Krzysztof Zaraska, Katarina Cvejin, Jan Kulawik, and Dorota Szwagierczak. 2016. "Development and Characterization of Miniaturized LTCC PH Sensors with RuO2 Based Sensing Electrodes." *Sensors and Actuators B: Chemical* 223:641–49.

Manjakkal, Libu, Dorota Szwagierczak, and Ravinder Dahiya. 2020. "Metal Oxides Based Electrochemical PH Sensors: Current Progress and Future Perspectives." *Progress in Materials Science* 109:100635.

Manjakkal, Libu, Krzysztof Zaraska, Katarina Cvejin, Jan Kulawik, and Dorota Szwagierczak. 2016. “Potentiometric RuO2–Ta2O5 PH Sensors Fabricated Using Thick Film and LTCC Technologies.” *Talanta* 147:233–40.

Matthews, D. R., R. R. Holman, E. Bown, J. Steemson, A. Watson, and S. Hughes. 1987. “Pen-Sized Digital 30-Second Blood Glucose Meter.” *Lancet (British Edition)* 1(8536):778–79.

McMurray, H. Neil, Peter Douglas, and Duncan Abbot. 1995. “Novel Thick-Film PH Sensors Based on Ruthenium Dioxide-Glass Composites.” *Sensors and Actuators B: Chemical* 28(1):9–15.

Moonen, Pieter F., Iryna Yakimets, and Jurriaan Huskens. 2012. “Fabrication of Transistors on Flexible Substrates: From Mass-Printing to High-Resolution Alternative Lithography Strategies.” *Advanced Materials (Deerfield Beach, Fla.)* 24(41):5526–41. doi: 10.1002/adma.201202949.

Mulchandani, Ashok, and Nosang V. Myung. 2011. “Conducting Polymer Nanowires-Based Label-Free Biosensors.” *Current Opinion in Biotechnology* 22(4):502–8.

Naumann, Renate, Ch Alexander-Weber, R. Eberhardt, J. Giera, and P. Spitzer. 2002. “Traceability of PH Measurements by Glass Electrode Cells: Performance Characteristic of PH Electrodes by Multi-Point Calibration.” *Analytical and Bioanalytical Chemistry* 374(5):778–86.

Nyein, Hnin Yin Yin, Wei Gao, Ziba Shahpar, Sam Emaminejad, Samyuktha Challa, Kevin Chen, Hossain M. Fahad, Li-Chia Tai, Hiroki Ota, and Ronald W. Davis. 2016. “A Wearable Electrochemical Platform for Noninvasive Simultaneous Monitoring of Ca2+ and PH.” *ACS Nano* 10(7):7216–24.

Park, Hong Jun, Jo Hee Yoon, Kyoung G. Lee, and Bong Gill Choi. 2019a. “Potentiometric Performance of Flexible PH Sensor Based on Polyaniline Nanofiber Arrays.” *Nano Convergence* 6(1):1–7.

Park, Hong Jun, Jo Hee Yoon, Kyoung G. Lee, and Bong Gill Choi. 2019b. “Potentiometric Performance of Flexible PH Sensor Based on Polyaniline Nanofiber Arrays.” *Nano Convergence* 6(1):9. doi: 10.1186/s40580-019-0179-0.

Parrilla, Marc, Inmaculada Ortiz-Gómez, Rocío Cánovas, Alfonso Salinas-Castillo, María Cuartero, and Gastón A. Crespo. 2019. “Wearable Potentiometric Ion Patch for On-Body Electrolyte Monitoring in Sweat: Toward a Validation Strategy to Ensure Physiological Relevance.” *Analytical Chemistry* 91(13):8644–51.

Patolsky, Fernando, and Charles M. Lieber. 2005. “Nanowire Nanosensors.” *Materials Today* 8(4):20–28.

Qin, Yiheng, Hyuck-Jin Kwon, Matiar MR Howlader, and M. Jamal Deen. 2015. "Microfabricated Electrochemical PH and Free Chlorine Sensors for Water Quality Monitoring: Recent Advances and Research Challenges." *RSC Advances* 5(85):69086–109.

Raja, Pandian Bothi, Kabilashen Readdyi Munusamy, Veeradasan Perumal, and Mohamad Nasir Mohamad Ibrahim. 2022. "5 - Characterization of Nanomaterial Used in Nanobioremediation." Pp. 57–83 in *Nano-Bioremediation : Fundamentals and Applications*, *Micro and Nano Technologies*, edited by H. M. N. Iqbal, M. Bilal, and T. A. Nguyen. Elsevier.

Renedo, O. Dominguez, M. A. Alonso-Lomillo, and MJ Arcos Martínez. 2007. "Recent Developments in the Field of Screen-Printed Electrodes and Their Related Applications." *Talanta* 73(2):202–19.

Rérolle, Victoire MC, Cedric FA Floquet, Matt C. Mowlem, Douglas P. Connelly, Eric P. Achterberg, and Richard RGJ Bellerby. 2012. "Seawater-PH Measurements for Ocean-Acidification Observations." *TrAC Trends in Analytical Chemistry* 40:146–57.

Robinson, Kay L., and Nathan S. Lawrence. 2006. "A Vinylanthracene and Vinylferrocene-Containing Copolymer: A New Dual PH/Sulfide Sensor." *Electroanalysis: An International Journal Devoted to Fundamental and Practical Aspects of Electroanalysis* 18(7):677–83.

Secor, Ethan. 2018. "Principles of Aerosol Jet Printing." *Flexible and Printed Electronics* 3. doi: 10.1088/2058-8585/aace28.

Sharma, Asha, Aamir Ahmed, Anoop Singh, Sai Kiran Oruganti, Ajit Khosla, and Sandeep Arya. 2021. "Recent Advances in Tin Oxide Nanomaterials as Electrochemical/Chemiresistive Sensors." *Journal of the Electrochemical Society* 168(2):027505.

Shi, Patrick, Xuechuan Shan, G. Tarapata, Ryszard Jachowicz, J. Weremczuk, and Hontat Hui. 2011. "Fabrication of Wireless Sensors on Flexible Film Using Screen Printing and via Filling." *Microsystem Technologies* 17:661–67. doi: 10.1007/s00542-010-1161-2.

Shinwari, M. Waleed, David Zhitomirsky, Imran A. Deen, P. R. Selvaganapathy, M. Jamal Deen, and D. Landheer. 2010. "Microfabricated Reference Electrodes and Their Biosensing Applications." *Sensors (Basel, Switzerland)* 10(3):1679–1715. doi: 10.3390/s100301679.

Sibug-Torres, Sarah May, Lance P. Go, and Erwin P. Enriquez. 2020. "Fabrication of a 3D-Printed Porous Junction for Ag|AgCl|gel-KCl Reference Electrode." *Chemosensors* 8(4):130. doi: 10.3390/chemosensors8040130.

Siden, Johan, and Hans-Erik Nilsson. 2007. "Line Width Limitations of Flexographic-Screen- and Inkjet Printed RFID Antennas." Pp. 1745–48 in *2007 IEEE Antennas and Propagation Society International Symposium*.

Simić, Mitar, Libu Manjakkal, Krzysztof Zaraska, Goran M. Stojanović, and Ravinder Dahiya. 2016. “TiO 2-Based Thick Film PH Sensor.” *IEEE Sensors Journal* 17(2):248–55.

Søndergaard, Roar R., Markus Hösel, and Frederik C. Krebs. 2013. “Roll-to-Roll Fabrication of Large Area Functional Organic Materials.” *Journal of Polymer Science Part B: Polymer Physics* 51(1):16–34.

Song, Edward, and Jin-Woo Choi. 2014. “Self-Calibration of a Polyaniline Nanowire-Based Chemiresistive PH Sensor.” *Microelectronic Engineering* 116:26–32. doi: 10.1016/j.mee.2013.10.014.

Suganuma, Katsuaki. 2014. *Introduction to Printed Electronics*. Vol. 74. Springer Science & Business Media.

Tang, Yitian, Lijie Zhong, Wei Wang, Ying He, Tingting Han, Longbin Xu, Xiaocheng Mo, Zhenbang Liu, Yingming Ma, Yu Bao, Shiyu Gan, and Li Niu. 2022. “Recent Advances in Wearable Potentiometric PH Sensors.” *Membranes* 12(5):504. doi: 10.3390/membranes12050504.

Tobjörk, Daniel, and Ronald Österbacka. 2011. “Paper Electronics.” *Advanced Materials* 23(17):1935–61.

Tortorich, Ryan P., Edward Song, and Jin-Woo Choi. 2013. “Inkjet-Printed Carbon Nanotube Electrodes with Low Sheet Resistance for Electrochemical Sensor Applications.” *Journal of The Electrochemical Society* 161(2):B3044.

Turunen, Robert, Dominique Numakura, M. Nakayama, and H. Kawasaki. 2008. “Screen Printing Process for High Density Flexible Electronics.” Pp. 44–49 in *Proc. IPC Printed Circuit Expo/APEX*.

Vasilescu, Alina, Gilvanda Nunes, Akhtar Hayat, Usman Latif, and Jean-Louis Marty. 2016. “Electrochemical Affinity Biosensors Based on Disposable Screen-Printed Electrodes for Detection of Food Allergens.” *Sensors* 16(11):1863.

Vidal, Juan-Carlos, Esperanza Garcia-Ruiz, and Juan-Ramón Castillo. 2003. “Recent Advances in Electropolymerized Conducting Polymers in Amperometric Biosensors.” *Microchimica Acta* 143(2):93–111.

Walker, Corey E., Zheng Xia, Zachary S. Foster, Brent J. Lutz, and Z. Hugh Fan. 2008. “Investigation of Airbrushing for Fabricating Microelectrodes in Microfluidic Devices.” *Electroanalysis: An International Journal Devoted to Fundamental and Practical Aspects of Electroanalysis* 20(6):663–70.

Wang, Joesph, Prasad Pamidi, and K. Rogers. 1998. “Sol - Gel-Derived Thick-Film Amperometric Immunosensors.” *Analytical Chemistry* 70:1171–75. doi: 10.1021/ac971093e.

Wang, Ren, Qingfeng Zhai, Yunmeng Zhao, Tiance An, Shu Gong, Zhirui Guo, QianQian Shi, Zijun Yong, and Wenlong Cheng. 2020. "Stretchable Gold Fiber-Based Wearable Electrochemical Sensor toward PH Monitoring." *Journal of Materials Chemistry. B* 8(16):3655–60. doi: 10.1039/c9tb02477h.

Wei, Di, Tom Lindfors, Carita Kvarnström, Leif Kronberg, Rainer Sjöholm, and Ari Ivaska. 2005. "Electrosynthesis and Characterisation of Poly(N-Methylaniline) in Organic Solvents." *Journal of Electroanalytical Chemistry* 575(1):19–26. doi: 10.1016/j.jelechem.2004.08.018.

Wen, Yugeng, Yunqi Liu, Yunlong Guo, Gui Yu, and Wenping Hu. 2011. "Experimental Techniques for the Fabrication and Characterization of Organic Thin Films for Field-Effect Transistors." *Chemical Reviews* 111(5):3358–3406. doi: 10.1021/cr1001904.

Wildgoose, Gregory G., Craig E. Banks, Henry C. Leventis, and Richard G. Compton. 2006. "Chemically Modified Carbon Nanotubes for Use in Electroanalysis." *Microchimica Acta* 152(3):187–214.

Wildgoose, Gregory G., Malingappagari Pandurangappa, Nathan S. Lawrence, Li Jiang, Timothy GJ Jones, and Richard G. Compton. 2003. "Anthraquinone-Derivatised Carbon Powder: Reagentless Voltammetric PH Electrodes." *Talanta* 60(5):887–93.

Xiang, Chen, Liangchao Li, Suyong Jin, Baiqun Zhang, Haisheng Qian, and Guoxiu Tong. 2010. "Expanded Graphite/Polyaniline Electrical Conducting Composites: Synthesis, Conductive and Dielectric Properties." *Materials Letters* 64(11):1313–15.

Xu, Bin, and Wei-De Zhang. 2010. "Modification of Vertically Aligned Carbon Nanotubes with RuO2 for a Solid-State PH Sensor." *Electrochimica Acta* 55(8):2859–64.

Xu, Shuaikai, Yohan Dall'Agnese, Guodong Wei, Chao Zhang, Yury Gogotsi, and Wei Han. 2018. "Screen-Printable Microscale Hybrid Device Based on MXene and Layered Double Hydroxide Electrodes for Powering Force Sensors." *Nano Energy* 50:479–88.

Yang, Jiang, Tae Joon Kwak, Xiaodong Zhang, Robert McClain, Woo-Jin Chang, and Sundaram Gunasekaran. 2016. "Digital PH Test Strips for In-Field PH Monitoring Using Iridium Oxide-Reduced Graphene Oxide Hybrid Thin Films." *Acs Sensors* 1(10):1235–43.

Yang, Yuxin, Xiaofei Wei, Nannan Zhang, Juanjuan Zheng, Xing Chen, Qian Wen, Xinxin Luo, Chong-Yew Lee, Xiaohong Liu, Xingcai Zhang, Jun Chen, Changyuan Tao, Wei Zhang, and Xing Fan. 2021. "A Non-Printed Integrated-Circuit Textile for Wireless Theranostics." *Nature Communications* 12(1):4876. doi: 10.1038/s41467-021-25075-8.

Yoon, Jo Hee, Kyung Hoon Kim, Nam Ho Bae, Gap Seop Sim, Yong-Jun Oh, Seok Jae Lee, Tae Jae Lee, Kyoung G. Lee, and Bong Gill Choi. 2017. "Fabrication of Newspaper-Based Potentiometric Platforms for Flexible and Disposable Ion Sensors." *Journal of Colloid and Interface Science* 508:167–73. doi: 10.1016/j.jcis.2017.08.036.

Zamora, M. L., J. M. Dominguez, R. M. Trujillo, C. B. Goy, M. A. Sánchez, and R. E. Madrid. 2018. "Potentiometric Textile-Based PH Sensor." *Sensors and Actuators B: Chemical* 260:601–8. doi: 10.1016/j.snb.2018.01.002.

Zhao, Rongrong, Meizhu Xu, Jian Wang, and Guonan Chen. 2010. "A PH Sensor Based on the TiO2 Nanotube Array Modified Ti Electrode." *Electrochimica Acta* 55(20):5647–51.

Zhou, Rui, Jun Li, Hongwei Jiang, Hui Li, Yao Wang, Danick Briand, Malick Camara, Guofu Zhou, and Nico F. de Rooij. 2019. "Highly Transparent Humidity Sensor with Thin Cellulose Acetate Butyrate and Hydrophobic AF1600X Vapor Permeating Layers Fabricated by Screen Printing." *Sensors and Actuators B: Chemical* 281:212–20.